MID-AMERICA TRANSPORTATION CENTER

Final Report
WBS: 25-1121-3002-104
Report # MATC: 104

Collaborative Last-Mile Delivery with Drones in Rural America

Shakiba Enayati, PhD
Assistant Professor (PI)
Supply Chain and Analytics Department
University of Missouri-Saint Louis

Pardis Bahmani, PhD Student
Research Assistant (co-author)
Supply Chain and Analytics Department
University of Missouri-Saint Louis

2025

A Cooperative Research Project sponsored by the U.S. Department of Transportation-Office of the Assistant Secretary for Research and Technology.

Collaborative Last-Mile Delivery with Drones in Rural America

Shakiba Enayati, Ph.D.
Assistant Professor (PI)
Supply Chain and Analytics Department
University of Missouri-Saint Louis

Pardis Bahmani, Ph.D. Student
Research Assistant (co-author)
Supply Chain and Analytics Department
University of Missouri-Saint Louis

A Report on Research Sponsored by

Mid-America Transportation Center

University of Nebraska–Lincoln

March 2025

Technical Report Documentation Page

1. Report No. 25-1121-3002-104	2. Government Accession No.	3. Recipient's Catalog No.	
4. Title and Subtitle Collaborative Last-Mile Delivery with Drones in Rural America		5. Report Date January 2025	
		6. Performing Organization Code	
7. Author(s) Shakiba Enayati ORCID No. 0000-0003-2586-7439 Pardis Bahmani		8. Performing Organization Report No. 25-1121-3002-104	
9. Performing Organization Name and Address Mid-America Transportation Center Prem S. Paul Research Center at Whittier School 2200 Vine St. Lincoln, NE 68583-0851		10. Work Unit No. (TRAIS)	
		11. Contract or Grant No. 69A3552348307	
12. Sponsoring Agency Name and Address Office of the Assistant Secretary for Research and Technology 1200 New Jersey Ave., SE Washington, D.C. 20590		13. Type of Report and Period Covered June 2023- December 2024	
		14. Sponsoring Agency Code	
15. Supplementary Notes			

16. Abstract

This report presents an optimization framework to improve rural healthcare logistics by integrating multi-modal transportation networks, including drones and ground vehicles. The framework addresses challenges such as high costs, excessive travel distances, and inefficiencies in uncoordinated systems. A novel weather-aware optimization model, incorporating a predictive function for energy consumption based on weather and time of arrival, ensures safer and more reliable drone operations. By leveraging advanced optimization techniques, the framework achieves cost reductions of up to 99% and reduces travel distances by over 88%.

A case study validating the model focuses on centralized delivery of test kits, demonstrating significant improvements in cost and distance compared to a decentralized baseline. The research explores scenarios involving single and multi-vehicle configurations, drone integration, and weather-aware systems. These findings highlight the value of centralized planning, predictive modeling, and drone integration, providing actionable insights for healthcare logistics and other sectors like disaster response and agriculture.

17. Key Words Rural Healthcare Logistics, Multi-Modal Transportation, Drone Integration, Optimization Modeling, Operational Efficiency.	18. Distribution Statement		
19. Security Classif. (of this report) Unclassified	20. Security Classif. (of this page) Unclassified	21. No. of Pages 96	22. Price

Table of Contents

List of Figures

List of Tables

Acknowledgments

We would like to express our heartfelt gratitude to Dr. Ziteng Wang from the College of Engineering and Engineering Management at Northern Illinois University and Dr. Sina Ansari from the Driehaus College of Business at DePaul University for providing the case study that served as a foundation for this research. Their valuable contributions were instrumental in shaping this work.

We also extend our sincere thanks to Dr. Srikanth Gururajan from the Department of Mechanical Engineering at Saint Louis University for his expertise in drones and his critical role in calculating drone energy consumption. His insights and guidance significantly enhanced the accuracy and robustness of our analysis.

This research would not have been possible without their generous support and collaboration, and we are deeply appreciative of their contributions.

Disclaimer

The contents of this report reflect the views of the authors, who are responsible for the facts and the accuracy of the information presented herein. This document is disseminated in the interest of information exchange. The report is funded, partially or entirely, by a grant from the U.S. Department of Transportation's University Transportation Centers Program. However, the U.S. Government assumes no liability for the contents or use thereof.

Abstract

This report presents an optimization framework designed to enhance rural healthcare logistics through the integration of multi-modal transportation networks, including drones and ground vehicles. The study focuses on improving the delivery of medical supplies from decentralized pick-up locations to a set of identical destination locations in a centralized manner, addressing challenges such as high transportation costs, excessive travel distances, and inefficiencies in uncoordinated systems.

A novel model is developed that integrates a predictive function of weather-based energy consumption into the optimization framework. This weather-aware modeling approach ensures safer and more reliable drone operations by accounting for energy consumption variations based on weather conditions and time of arrival at a location. By leveraging optimization modeling, the proposed framework achieves cost reductions of up to 99% and reduces total travel distances by over 88%. Drones, integrated into the delivery network, enable efficient workload distribution, faster deliveries, and improved accessibility in regions with limited infrastructure.

A case study forms the foundation of validating the proposed model, focusing on the centralized delivery of test kits from multiple locations to a lab. By optimizing routes, schedules, and resource allocation, the study demonstrates significant reductions in operational costs as well as delivery times compared to the baseline decentralized delivery system.

The research evaluates several scenarios, including single-vehicle operations, multi-vehicle configurations, and drone integration, as well as comparisons between weather-aware and non-weather-aware models. The results highlight the trade-offs between cost-efficiency and reliability, with weather-aware systems offering enhanced safety and predictability despite marginally higher costs.

This study provides actionable insights for decision-makers, emphasizing the transformative potential of centralized planning, multi-modal transportation systems, and predictive modeling integrated with optimization techniques. The findings address critical transportation and logistical challenges in healthcare, offering a scalable framework for redesigning delivery networks to ensure efficiency, equity, and accessibility. These insights extend beyond healthcare to inform transportation solutions in other sectors, such as disaster response and agriculture, underscoring the importance of innovative approaches in resource-constrained and disruption-prone environments.

Chapter 1 Introduction

1.1 Background and Motivation

The healthcare supply chain is a cornerstone of global health systems, facilitating the timely delivery and accessibility of essential medical supplies and medications to healthcare facilities worldwide (Kruk et al., 2018). A well-functioning healthcare supply chain is indispensable for building sustainable, efficient, and equitable health systems, which are critical for global health security and human survival (Backman et al., 2008). Despite its significance, the healthcare supply chain is fraught with challenges, particularly in rural and underserved areas. Inadequate infrastructure, difficult terrains, traffic congestion, and high vehicle maintenance costs undermine the reliability of traditional truck-based delivery methods (Wang et al., 2022). These barriers perpetuate disparities in healthcare access, leaving vulnerable communities at heightened risk. Addressing these inequities requires innovative approaches that enhance delivery efficiency, resilience, and equity in resource distribution.

Rural areas, where over 60 million people—roughly one-fifth of the U.S. population—reside, exemplify the acute challenges of last-mile healthcare delivery (Douthit et al., 2015). These regions face unique difficulties, including geographic isolation and limited transportation infrastructure, that amplify the barriers outlined in the broader healthcare supply chain context (Skillman et al., 2010). Lengthy distances, rugged terrains, and severe weather conditions further complicate the delivery of essential medical resources, frequently resulting in delays in providing life-saving medications, vaccines, and equipment (Morris et al., 2022). Addressing the challenges in rural healthcare delivery is not only critical for reducing health disparities but also for ensuring the resilience of the healthcare system during emergencies, such as pandemics, when rapid and efficient supply chain solutions are paramount.

Technological advancements in drone technology have shown immense potential to address the logistical barriers of last-mile delivery in healthcare supply chains (Jeon et al., 2022). Drones, or unmanned aerial vehicles (UAVs), are valued for their speed, flexibility, and environmentally friendly design, which enable them to navigate challenging environments such as rugged terrains and isolated regions (Lamptey and Serwaa, 2020; Griffith et al., 2023). By bypassing the limitations of traditional transport systems, drones can ensure timely delivery of critical medical supplies to underserved areas. Trends in logistics, including speed, sustainability, flexibility, and automation, highlight the transformative role of drones in reshaping last-mile delivery systems (Bosona, 2020; Lim et al., 2018).

Rural regions, where healthcare access is hindered by inadequate transportation infrastructure, long distances, and severe weather, stand to benefit significantly from drone-enabled delivery. These systems can overcome logistical challenges and improve access to essential resources such as medications, vaccines, and life-saving equipment. Research has demonstrated the feasibility and benefits of using drones for healthcare delivery during emergencies like the COVID-19 pandemic, especially in rural medical centers (Sham et al., 2022). However, despite the growing interest in the use of drones for healthcare delivery, their practical integration into healthcare supply chains remains limited. Operating drones in dynamic and unpredictable environments poses significant challenges, with weather conditions emerging as a critical constraint (Dorling et al., 2017; Troudi et al., 2018). Adverse and variable weather, such as fluctuating wind speeds and directions, can disrupt drone missions by increasing energy consumption and limiting operational range (Thibbotuwawa et al., 2019). That said, favorable conditions, such as tailwinds aligned with a drone's flight path, can extend its range and efficiency.

Current solutions for drone integration often fail to address these operational constraints comprehensively, including flight range, payload capacity, and environmental factors such as wind and humidity (Chen et al., 2021; Zhang et al., 2021). To maximize the potential of drones in healthcare logistics, there is a critical need for robust optimization frameworks that consider these factors and the uncertainties in energy consumption. By addressing these gaps, drones can be more effectively deployed to enhance healthcare delivery in underserved rural areas, transforming access to critical medical resources and building resilient supply chains.

1.2 Objectives and Organization

This research is motivated by the transformative potential of integrating drones into medical supply chains and the need to address the gap in existing literature, which often overlooks the impact of realistic drone flight conditions. The study focuses on optimizing a multi-modal medical supply logistics network that combines drones and traditional ground vehicles for efficient and reliable transportation. By incorporating the influence of weather conditions (e.g., wind magnitude and direction) on vehicle performance, the proposed model aims to enhance the resilience and efficiency of healthcare supply chains, especially in resource-constrained and challenging environments.

The primary objective of the model is to minimize total supply chain costs, encompassing transportation and operational expenses within the medical logistics network. At the operational level, the model determines optimal decisions for locations of vehicle recharging/refueling during the delivery operation, designing delivery routes, identifying transshipment nodes, and scheduling pickup-and-delivery activities. Certain nodes in the network function as operational bases, serving as the starting and ending points for vehicle routes, with each vehicle required to begin and conclude its journey at its designated base. Although a single link is considered

between each pair of nodes for each transportation mode, the model allows for medical orders to be transferred between multiple vehicles, enabling seamless transshipment along the delivery route. This integration facilitates the efficient use of diverse transportation modes, improving overall system performance while addressing the unique challenges of medical supply logistics.

To account for realistic drone energy consumption into the proposed routing and scheduling optimization, the network is segmented into sub-regions using a Voronoi diagram based on weather station locations. This segmentation allows for precise energy estimation by incorporating weather conditions across the network. Using established formulas, energy consumption is calculated for various drone types, and a predictive function integrates dynamic weather forecasts to enhance planning accuracy. This predictive function is further embedded into the optimization modeling framework, enabling holistic decision-making for efficient and reliable operations while addressing energy constraints and environmental variability in drone-enabled healthcare delivery systems.

This research is driven by the need to enhance the efficiency, reliability, and resilience of medical supply chains through the integration of drone technology and ground transportation. It seeks to address key challenges by exploring the following research questions:

1. How can drone-enabled delivery systems be integrated with traditional ground transportation to optimize the efficiency and reliability of medical supply chains in rural and resource-constrained regions?
2. What is the impact of incorporating dynamic weather conditions, such as temperature, wind direction and magnitude, on drone energy consumption and the overall performance of the medical logistics network?

3. What are the optimal configurations for vehicle routing, including the locations to recharge/refuel vehicles, transshipment nodes, and delivery schedules, to minimize costs and maximize system resilience under uncertain environmental conditions?

The remainder of this report is organized as follows: Chapter 2 provides a comprehensive literature review, covering topics related to vehicle routing problems, drone delivery networks, and weather-aware drone delivery systems. Chapter 3 presents a detailed problem description and the proposed model formulation. Chapter 4 outlines the case study used to contextualize the research. Chapter 5 discusses the numerical results and analysis. Finally, Chapter 6 concludes the report with managerial insights, key findings, and suggestions for future research.

Chapter 2 Literature Review

This chapter presents a comprehensive literature review on the key components of our research problem, focusing on advancements and challenges in vehicle routing problems, the design and operational considerations of drone delivery logistics networks, and the integration of weather conditions into drone supply chain optimization models. Structured into three subsections, the review explores how these elements intersect in the context of healthcare logistics, addressing critical real-world constraints such as energy consumption, payload capacities, and environmental uncertainties. By analyzing the current state of the art, this chapter identifies significant research gaps in existing models, particularly in their ability to account for dynamic weather impacts on drone performance. The review concludes with a summary of these gaps and categorizes the most recent studies, highlighting their contributions, limitations, and relevance to the development of more robust and practical solutions for healthcare logistics optimization.

2.1 Vehicle Routing Problem and Key Features

The classical Vehicle Routing Problem (VRP) focuses on determining a set of minimum-cost routes for a fleet of vehicles to service customer demands, starting and ending at a central depot. These models assume a fixed set of vehicles and customers, with costs typically determined by distances between locations and fixed expenses associated with vehicle usage.

A notable extension of the classical VRP is the Pickup-and-Delivery Problem (PDP), which introduces additional complexity by requiring vehicles to handle paired customer requests for both pickups and deliveries. The objective in PDP is to design minimum-cost routes that satisfy all such requests while adhering to pairing constraints (Rais et al., 2014).

In many real-world logistics and transportation scenarios, time-sensitive services play a critical role (Naccache et al., 2018; Aziez et al., 2020). This necessity leads to the Vehicle Routing Problem with Time Windows (VRPTW), which incorporates constraints for time-specific pickups and deliveries. The integration of time windows adds practical relevance to VRP models, enabling their application to scenarios requiring precise scheduling and coordination.

Some studies in the literature extend the classical VRP by integrating transshipment capabilities, where payloads can be transferred between vehicles to enhance routing flexibility (Lyu and Yu, 2023). In pickup and delivery problems with transshipment, customer requests can be dropped off at designated transshipment stations for temporary storage. Other vehicles can subsequently pick up these requests to complete the delivery, improving efficiency and adaptability in complex logistics networks.

Recognizing the critical role of logistics networks in healthcare, several studies have focused on pharmaceutical distribution. For example, Campelo et al. (2019) developed a distribution network model that accommodates customers requiring multiple daily deliveries and different service-level agreements with time windows. Similarly, Liu et al. (2013) proposed two mixed-integer programming models for a vehicle routing problem with time windows and multiple pickups and deliveries to optimize home healthcare delivery from providers to customers.

Mahmoudi et al. (2019) introduced a mixed-integer programming model for a pickup and delivery problem with transfers, incorporating a continuous-time approximation approach using cumulative arrival, departure, and on-board count diagrams. Their model included a cumulative service state dimension to monitor parcel service status, enhancing system performance insights. Wolfinger (2021) further advanced this field by extending the pickup and delivery problem to

include time windows, split loads, and transshipments. This approach minimizes total network costs, including travel expenses and transshipment costs, while ensuring timely pickups and deliveries. The addition of split loads and transshipments provides practical adaptability, addressing real-world challenges such as resource constraints and dynamic customer demands in logistics networks. In our research, we incorporate the possibility of transshipment between vehicles, time windows for pickup and delivery, and paired pickup-and-delivery requests. These features allow for a more realistic and flexible approach to modeling and optimizing complex healthcare logistics networks.

2.2 Drone Delivery Networks

Recently, there has been growing interest in drone delivery logistics networks, with studies emphasizing their efficiency in reducing costs and saving time across various industries, including healthcare and humanitarian efforts (Zhang et al., 2023). For instance, Betti Sorbelli (2024) provided a comprehensive review of drone delivery networks and their applications, while Gunaratne et al. (2022) demonstrated the effectiveness of integrating drones into healthcare delivery in low-income regions. From a managerial perspective, Stolaroff et al. (2018) highlighted that precise implementation of drone-based delivery systems could significantly reduce greenhouse gas emissions and energy consumption in the freight sector.

Several researchers have developed optimization models to address drone routing problems, focusing on various operational aspects and objectives. Kim et al. (2021) proposed a routing algorithm to identify optimal round-trip routes for drones delivering goods from depots to customers, aiming to minimize total delivery distances while accounting for range and payload capacities. Similarly, Dorling et al. (2017) introduced two multi-trip VRP models for drone delivery: one minimizing costs within a time limit and the other reducing overall delivery time

under a budget constraint, both incorporating energy consumption affected by payload and battery weight. Other studies, such as those by Thibbotuwawa et al. (2019) and Radzki et al. (2019), focused on maximizing customer satisfaction by considering operational factors such as time, payload, and battery capacity.

Another branch of the literature has explored multi-modal logistics networks that integrate drones with traditional ground-based vehicles, enabling transshipment between modes of transportation. Kim et al. (2024) proposed a multi-modal logistics framework that combines the strengths of drones and vehicles for efficient delivery. Wolfinger et al. (2019) developed a multi-modal long-haul routing problem incorporating transshipment nodes and pickup and delivery time windows, demonstrating that combining short-haul vehicles with long-haul transportation can result in significant cost savings, particularly for long-distance deliveries. Enayati et al. (2023) introduced a strategic multi-modal vaccine distribution model, optimizing the locations of local distribution centers, drone bases, and relay stations while adhering to cold chain time limits and drone range constraints. These studies collectively highlight the potential of integrated logistics systems to address complex challenges in modern supply chains.

Addressing flight range limitations in drones, several studies have explored innovative solutions. Pinto and Lagorio (2022) examined the expansion of drones' operational range by designing networks with strategically positioned charging stations to enable in-route recharging. Tseng et al. (2017) analyzed drone battery performance under varying flight conditions, including motion, weight, and wind, and integrated recharging optimization into mission planning. Alyassi et al. (2023) developed a machine learning model to optimize energy-efficient and time-feasible tours, incorporating recharge scheduling to overcome battery limitations. Similarly, Dukkanci et al. (2021) proposed a mixed-integer nonlinear programming model to

minimize energy consumption and time-based operational costs in a drone delivery network, while Moadab et al. (2022) introduced a mixed-integer linear programming model that utilizes public transportation vehicles as mobile charging stations to enhance energy efficiency and delivery effectiveness.

Our research similarly considers drones as part of a multimodal transportation network. We address the limitations of drone payload capacity and flight range, as well as the necessity for appropriate operational bases for takeoff and landing. Furthermore, the flight range of drones can be extended through recharging or refueling stations along the route. Contrary to the general literature, we do not treat flight range as a fixed value. Instead, it is linked to the drone battery's energy consumption, which is influenced by weather predictions at the time of planning. The next section reviews relevant literature that incorporates weather conditions into the optimization of drone operation planning.

2.3 Weather-Responsive Optimization in Drone Supply Chains

Some researchers have investigated the barriers to adopting drone delivery systems (Koshta et al., 2024), identifying key challenges that distinguish drone delivery from traditional ground vehicle logistics. A notable challenge is the significant impact of weather conditions on drones' operational performance, including energy consumption (Beigi et al., 2022), flight range, and flight time. This has led to the development of specialized optimization models (Bocewicz et al., 2022).

Recent studies have incorporated weather effects, either directly or indirectly, into optimization frameworks to evaluate and enhance drone performance. For instance, Thibbotuwawa et al. (2019) provided a comprehensive analysis of the parameters affecting drone energy consumption in routing problems. Similarly, Palazzetti (2021) examined the impact of

windy conditions on energy consumption, emphasizing how detours from planned depots and routes influence distance traveled. Chen et al. (2023) addressed a vehicle routing problem by considering various wind scenarios to evaluate their effects on drone performance. Gürel and Serdarasan (2024) explored sustainable last-mile delivery by integrating wind into drone-assisted deliveries, analyzing their impact on delivery efficiency across varying scenarios.

Building on the soft time window VRP proposed by Guerriero et al. (2014) and the decision-support approach of Thibbotuwawa et al. (2019) for multi-trip fleet mission planning that accounts for weather dependencies, Radzki et al. (2019) extended a VRP by incorporating weather-dependent, non-linear energy consumption into a constraint programming framework using IBM ILOG. Their model addresses drone route planning under dynamic weather conditions and energy constraints, ensuring collision-free deliveries within specified time windows while maximizing customer satisfaction and the quantity of goods delivered. In another contribution, Cheng et al. (2024) proposed a two-period data-driven scheduling model for drone delivery systems. This model integrates uncertain flight times derived from wind observation data using a cluster-wise ambiguity set, aiming to minimize the essential riskiness index and enhance robustness against weather uncertainties. Initial schedules are determined in the first period, with the flexibility to adjust based on updated weather information in the second period.

To the best of our knowledge, no previous research has explicitly integrated energy consumption calculations and predictions into the optimization framework as we have done in this study.

2.4 Summary and Research Gap

While the reviewed literature highlights advancements in drone delivery networks, energy-efficient routing, and multi-modal logistics, gaps remain in developing models that

integrate multi-modal transportation, energy constraints, transshipment, and weather-aware drone delivery logistics networks, particularly in the medical supply area. Although prior studies have explored routing under energy limitations and weather dependencies, they often focus on the effects on flight range or delivery time schedules. Existing research has addressed various operational challenges such as the impact of battery capacity and payload, time window constraints, multi-modal networks, and transshipment operations on total network costs. Additionally, some studies have incorporated weather conditions, particularly wind, to assess their influence on delivery schedules, battery performance, and flight range. However, none have developed a weather-aware drone routing model that explicitly considers drone energy consumption as a function of flight time. Table 2.1 summarizes the seminal literature and highlights the research gap that this study aims to address. The following abbreviations are used in Table 2.1: TC represents total cost, DT stands for delivery time, TT is travel time, TD denotes traveled distance, EC refers to energy consumption, R is the risk of late delivery, CS signifies customer satisfaction, and NV indicates the number of used vehicles.

This research aims to minimize the total cost of delivery operations in a multi-modal network, including transportation, recharging, and transshipment costs. It does so by optimizing routes, selecting recharging station locations, identifying transshipment nodes, and scheduling pickups and deliveries, while accounting for vehicles' energy consumption, particularly focusing on drones affected by weather conditions. The study offers a linear optimization formulation that facilitates the transshipment of orders between vehicles along the route, considering the time windows for pickups and deliveries, and vehicle capacities. Notably, it is the first model to explicitly incorporate drone energy consumption predictions into the optimization framework. The next section describes the problem and presents the proposed formulation.

Table 2.1 Summary of the most relevant studies

	Reference	Objective Function	Model Type	Network Setup			Transportation Mode		Operational Constraints				Solution Approach
				Transshipment Nodes	Pickup Locations	Recharge Stations	Drone	Conventional	Wind	Energy Capacity	Time Window	Vehicle Capacity	
1	F. Guerriero et al(2014)	Min TD, Max ACS, Min NV	Non-linear				*				*		Heuristics
2	Dorling et al(2016)	Min TC, Min DT	Linear				*			*	*	*	Exact
3	Tseng et al(2017)	Min TT	Linear			*				*	*		Exact
4	Wolfinger et al(2018)	Min TC	Linear	*	*			*			*	*	Heuristics
5	Thibbotuwawa et al(2019)	Max CDF	Non-linear		*		*		*	*	*	*	Heuristics
6	RADZKI(2019)	Max CS	Non-linear		*		*		*	*	*	*	Heuristics
7	Dukkanci(2021)	Min TC	Non-linear		*		*			*	*		Exact
8	Palazzetti(2021)	Min TD	Linear				*		*	*			Exact
9	Kim et al(2021)	Min TD	Linear		*		*					*	Exact
10	Moadab et al(2022)	Min EC	Linear		*	*	*			*			Exact
11	Alyassi et al(2022)	Min TT	Linear		*	*	*			*	*		Heuristics
12	Bocewics et al.(2022)	Min TT	Non-linear		*		*		*	*	*	*	Heuristics
13	Chen et al(2023)	Min TC	Linear		*		*		*	*	*	*	Heuristics
14	Enayati et al(2023)	Min TC	Linear		*	*	*	*		*		*	Exact
15	Cheng et al(2024)	Min R	Linear		*		*		*	*	*		Exact
16	Gurel et al(2024)	Min TT	Linear		*		*		*		*	*	Exact
17	This study(2024)	Min TC	Linear	*	*	*	*	*	*	*	*	*	Exact

Chapter 3 Problem Description and Model Formulation

3.1 Problem Definition

This study addresses the problem of routing and scheduling orders generated at a set of pickup locations to be delivered to identical destinations. The service network consists of nodes representing various geographical locations and multi-modal links to efficiently transport medical supplies. Nodes can serve multiple functions, such as being both an operational base for a vehicle and a pickup site.

Pickup locations have orders, and destinations are identical, meaning each pickup site can send their orders to one of the existing destinations based on the optimal route selected by the model. The network includes multiple transportation modes, such as traditional ground vehicles and various types of drones, each with a fleet of identical vehicles. Each mode can traverse the corresponding links in the network based on availability. A pair of nodes can be connected by multiple transportation modes, such as a truck and a small drone, each representing a different link. However, there is only one link per transportation mode between each pair of nodes.

Certain nodes within the network function as operational bases, serving as the starting and ending points for vehicle routes. Each vehicle must start and end its journey at its assigned operational base after delivering orders and completing its route. Medical orders can also be transferred between multiple vehicles at designated transshipment nodes along the delivery route if needed.

Furthermore, the network includes recharging/refueling stations for each mode of transportation, allowing vehicles to replenish energy along their routes. To ensure continuous and reliable operation, vehicle paths are closely monitored to maintain energy levels above a specified threshold. For drones, this may involve rapid battery swaps conducted by personnel,

effectively restoring the drone's energy capacity. Cars are refueled/recharged at the nearest gas/electric stations. This ensures efficient, reliable, and uninterrupted delivery operations.

The goal is to minimize total supply chain costs, including transportation, recharging, and transshipment operations, by optimizing routes, selecting recharging station locations, identifying transshipment nodes, and scheduling pickups and deliveries while accounting for the energy consumption of vehicles en route. For ground vehicles, like cars, energy consumption can be calculated by considering their miles per gallon (MPG). By multiplying the MPG by the travel distance, we can estimate the fuel consumed. For instance, if a car travels 50 miles and has an MPG of 25, the energy consumed would be approximately two gallons of fuel. This estimation can be adjusted based on travel time, taking into account variations in driving conditions and fuel efficiency. For drones, we propose an approach to integrate the prediction of energy consumption based on time-dependent weather forecasts into the optimization model—see Section 3.3 for more details.

3.2 Assumptions

The following assumptions provide the foundation for the model, ensuring it captures the critical aspects of operational and practical constraints in medical supply delivery. These assumptions reflect real-world conditions to achieve realistic and implementable solutions.

Pickup and Delivery Configurations. Each order is constrained by a time window, meaning pickups must occur after the earliest pickup time at the designated location and deliveries must be completed before the latest delivery time at the destination. Each destination has a limited capacity to handle only a certain number of orders at any given time.

Transportation Modes. The availability of vehicles for each mode of transportation (e.g., ground vehicles, drones) is predefined, and each vehicle has fixed payload and energy

capacities. Vehicles must be recharged or refueled once their energy capacity falls below a predefined safety threshold, ensuring uninterrupted operations and mitigating the risk of disruptions.

Operational Bases. All vehicles must begin and end their routes at their designated operational bases. For instance, drones must launch from and land at specific drone bases. This ensures consistent vehicle management and tracking throughout their routes and aligns with the practicalities of fixed base locations within a static service region.

Recharge Stations. Vehicles are assumed to start fully charged at the beginning of each planning period when departing from their operational bases. During operations, vehicles such as cars can recharge to their maximum capacity at the nearest gas or charging station. For drones, spare batteries are available at recharging stations, enabling quick battery swaps performed by trained personnel. This is to ensure that drones can quickly resume operations, minimizing downtime. A fixed amount of time is assumed for recharging or battery swapping for all vehicle types, irrespective of the station's location.

Energy Consumption. For traditional ground vehicles, energy consumption is calculated based on fuel efficiency (e.g., miles per gallon) and travel distance. For drones, energy consumption depends on time and is influenced by weather conditions. At the beginning of the planning period, weather predictions are used to update the drones' time-based energy consumption matrix, ensuring the model captures the effects of prevailing weather, such as wind, on energy requirements. The energy consumed when traversing an arc is modeled as a function of the arrival time at a location and serves as an input to the optimization model. It is assumed that the energy consumption prediction model is accurate and provides reliable inputs for planning.

Battery Performance Degradation. Drone battery performance is assumed to remain constant for the duration of the planning horizon. Any degradation in battery efficiency over time or due to repeated charging cycles is not accounted for.

Transshipment locations. Designated handoff points between ground vehicles and drones are given. These locations are equipped with the necessary infrastructure for safe loading and unloading of supplies. Also, drones and ground vehicles are assumed to be fully compatible with the handoff infrastructure, ensuring smooth and efficient transitions between transportation modes.

Demand Variability. Demand for medical supplies at each location is assumed to be known in advance and static for the planning period. Seasonal or unexpected surges in demand are not considered in the current model.

Cost Considerations. It is assumed that the service region is supported by shared resources, including ground vehicles and drones of multiple types, operated by third-party logistics providers. These operators account for variable costs such as operator fees, vehicle maintenance, infrastructure expenses, and other operational overheads. For modeling simplicity, all these costs are consolidated and represented as variable costs measured in terms of $/time unit.

Planning Horizon. The decisions are assumed to be made at the operational level, covering a finite period during which all orders must be delivered. This timeframe is designed to align with the immediate and time-sensitive nature of medical supply deliveries, ensuring that demand is met efficiently within the specified duration.

3.3 Drone Energy Consumption Calculation

We calculate the weather-based energy consumption for every drone arc at various times throughout the planning horizon (e.g., hourly). Accurate energy consumption estimation is critical for operational planning and depends on the dynamic weather conditions affecting drone performance. To incorporate localized weather variations, the service region is divided into Voronoi regions (VRs), with each region representing the area influenced by a specific weather station. These weather stations act as seed points, defining boundaries such that every location within a Voronoi region is closer to its respective weather station than to any other station (see Figure 3.1).

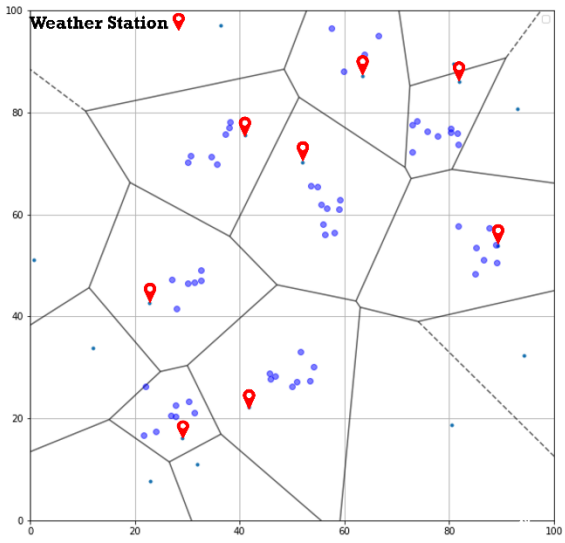

Figure 3.1 Discretization of service area using Voronoi regions

Weather data (including temperature, wind magnitude, and wind direction, etc.) is reported by these weather stations at regular intervals (e.g., hourly). Since weather information is not available for every individual location in the service area, the conditions observed at the weather station are used as a proxy for all locations within its corresponding VR. This

partitioning ensures that the weather conditions applied in the energy calculations reflect localized variations across the service region.

Each drone arc is analyzed based on its trajectory through the Voronoi regions. Two types of arcs are identified:

1. **Arcs Fully Contained Within a Single Voronoi Region:** For arcs whose endpoints lie within the same VR, energy consumption is calculated directly using the weather data reported for that region at the corresponding time interval.
2. **Interregional Arcs Crossing Multiple Voronoi Regions:** For arcs with endpoints in different VRs, the arc is divided into segments at the points where it crosses regional boundaries (see Figure 3.2). Each segment is assigned to the weather conditions of the VR it traverses, and the energy consumption for the entire arc is calculated by summing the energy consumed for all its segments. This segmentation ensures that energy consumption calculations account for spatial weather variations as the drone crosses multiple regions.

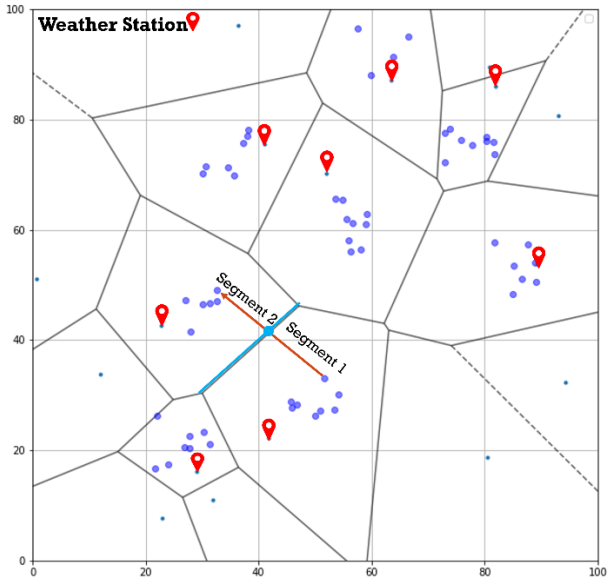

Figure 3.2 Creating segments on different Voronoi regions for interregional arcs

In this research, we only consider wind magnitude and direction collected from every weather station in the service area. To calculate the energy consumed for steady-level drone flight, we use the formula (D'Andrea, 2014): $EPM_t = \frac{1}{1-\Phi_t}\left(\frac{mg}{r\eta}\right)$, where EPM_t refers to the energy consumed per mile at time *t,* Φ_t denotes the ratio of headwind to airspeed, capturing the impact of wind resistance, m corresponds to the drone mass including its battery weight and payload, g is the acceleration of gravity, r denotes unitless lift to drag ratio reflecting aerodynamic efficiency, and η corresponds to the battery and motor power transfer efficiency. This formula incorporates key factors that influence energy consumption, including the drone's weight, aerodynamic properties, and the effect of wind. To ensure a conservative approach, we assume the drone is fully loaded during calculations, representing the highest possible energy consumption for a given arc.

The energy consumption for each arc is computed at every time interval during the planning horizon based on the reported weather conditions. For interregional arcs, segment-level

energy consumption is calculated for each VR using the localized weather data, and the total energy consumed is obtained by summing the energy for all segments. By integrating spatial and temporal weather variations, this method enables precise and reliable energy consumption estimation for drone operations, ensuring efficient route planning and robust performance across the service region.

Hence, for each drone arc in the network, energy consumption is calculated for every discretized time interval (e.g., hourly) by considering the arc's direction relative to the wind's magnitude and direction during that specific time. This process generates a time series of energy consumption values for each arc throughout the planning horizon. These time series data capture the dynamic influence of weather conditions on energy usage, allowing for a detailed understanding of how weather impacts drone performance over time.

To integrate this information into the optimization model presented in Section 3.5, a prediction function is fitted to the time series data. This function ($\mathcal{E}_{jk}^{v}(\mathcal{T}'_{jv})$, see Table 3.2) estimates the energy consumption on each arc as a continuous function of time, providing an essential input for the optimization process. The chosen prediction function must offer an explicit and computationally efficient representation of the energy-time relationship to support the model's performance. Importantly, the functional form of the prediction model, along with its parameters, is treated as a fixed parameter of the optimization model. However, the energy consumption is ultimately defined based on a decision variable: the departure time from a node. This ensures that the model dynamically incorporates energy variations as determined by the time-dependent nature of drone operations.

In this research, we apply a linear regression model as the prediction function. A linear function simplifies the computational complexity, especially when used in the mixed-integer

linear programming (MILP) framework proposed in Section 3.5. Linear functions are computationally efficient and allow the optimization solver to handle the time-dependent energy constraints more effectively.

This approach highlights the dual role of the prediction function: (1) providing a compact, explicit representation of the energy consumption over time and (2) enabling efficient integration into the optimization model to determine optimal drone routes and schedules that account for weather-based energy usage. While other forms of prediction functions, such as nonlinear or machine learning models, could be explored in future work, the linear regression model serves as a practical and effective choice for the current study.

3.4 Description of Optimization Model Inputs

The medical supply logistic network under study is represented as a directed network including a set of discrete geographic coordination nodes, denoted by $\mathcal{S}$, which are interconnected by arcs in the set $\mathcal{A}$. Each arc in $\mathcal{A}$ is represented by a tuple (i, j, v), where node $i \in \mathcal{S}$ is connected to node $j \in \mathcal{S}$ via vehicle $v \in \mathcal{V}$. The set $\mathcal{V}$ indicates the available vehicles within the network, which include drones of possibly different types and ground transportation vehicles. The network includes four types of facility functionalities: (1) Operational bases for each vehicle $v \in \mathcal{V}$, where the vehicle must start and end its route, denoted by $\mathrm{O}^v \in \mathcal{S}$ and $\mathrm{O}'^v \in \mathcal{S}$, respectively; (2) Recharging stations for each vehicle $v \in \mathcal{V}$, where vehicles can be recharged to be able to continue their routes, represented by nodes in the set $\mathcal{P}^v$; (3) Pickup location $\mathrm{P}(r)$ for each order $r \in \mathcal{R}$, from which the order r must be picked up; and (4) Identical destination nodes, denoted by the set $\mathcal{D}$, where each order must be delivered to one of these nodes. Each node $i \in \mathcal{S}$ can correspond to one or more than one type of functionality, and the union is indicated by $\mathcal{S} = \{\mathrm{O}^v \cup \mathrm{O}'^v \cup \mathcal{P}^v \cup \mathrm{P}(r) \cup \mathcal{D}\}$.

Each order pickup location generates an order indicated by $r \in \mathcal{R}$ with a quantity of $\mathrm{Q}(r)$. The total amount of orders carried by a vehicle $v \in \mathcal{V}$ on its associated arcs cannot exceed the vehicle's capacity U_v. Additionally, each destination node $d \in \mathcal{D}$ can accept a maximum order volume of K_d and the total amount of orders delivered to it can not surpass this limit. The cost of transshipping orders on each arc $(i, j, v) \in \mathcal{A}$ is represented by C_{ijv}, which is directly related to the distance between nodes i and j. Parameters ω^v and λ indicate the costs associated with recharging vehicle $v \in \mathcal{V}$, and transshipping orders between vehicles at a location, respectively.

Each order $r \in \mathcal{R}$ has a specific time window to be picked up from location $\mathrm{P}(r)$, starting at $a_{\mathrm{P}(r)}$ as the earliest pickup time, and to be delivered to a destination $d \in \mathcal{D}$ before b_r as the latest order delivery time. Also, l_d indicates the latest time for any order to be delivered to the destination $d \in \mathcal{D}$. The parameter θ_{ijv} represents the travel time for vehicle $v \in \mathcal{V}$ on arc $(i, j, v) \in \mathcal{A}$, while h_{vn} indicates the time required to transship an order from vehicle $v \in \mathcal{V}$ to vehicle $n \in \mathcal{V}$. Each vehicle $v \in \mathcal{V}$ has a maximum energy capacity of $\mathrm{E}^v_{\max}$ and a minimum energy reserve requirement of $\mathrm{E}^v_{\min}$ to ensure operational safety. The energy consumed by a vehicle while traveling across the arc $(j, k, v) \in \mathcal{A}$ is a function of its departure time from node $j \in \mathcal{S}$ and is represented by $\mathcal{E}^v_{jk}\left(\mathcal{T}'_{jv}\right)$ (see Section 3.3 for more detail). The time required for recharging each vehicle $v \in \mathcal{V}$ is denoted by parameter g^v.

The decision variables of the model are all operational, including selection of arcs to make delivery routes, order shipments and transshipments, location and time of recharging operations, time scheduling of order deliveries and energy management of vehicles to ensure safe and reliable operations within the network. Binary variable $\mathcal{X}_{ijv}$ indicates whether arc $(i, j, v) \in \mathcal{A}$ is included in the route of vehicle $v \in \mathcal{V}$. The binary variable $\mathcal{Y}^r_{ijv}$ tracks whether order $r \in \mathcal{R}$

is carried on the arc $(i, j, v) \in \mathcal{A}$. Binary variable $\mathcal{Z}_{iv}$ demonstrates if vehicle $v \in \mathcal{V}$ is recharged at node $i \in \mathcal{P}^v$. Additionally, binary variable γ_{ir}^{vn} captures whether order $r \in \mathcal{R}$ is transshipped from vehicle $v \in \mathcal{V}$ to vehicle $n \in \mathcal{V}$ at node $i \in \mathcal{S}$, and variable δ_i indicates if at least one order is transshipped at node $i \in \mathcal{S}$. Time-related decision variables $\mathcal{T}_{iv}$ and $\mathcal{T}'_{iv}$ capture the arrival and departure times of vehicles $v \in \mathcal{V}$ at node $i \in \mathcal{S}$, respectively. Similarly, energy variables E_{iv} and E'_{iv} monitor the remaining energy of the vehicles upon arrival and departure at each node. The full notations for sets, parameters, and decision variables of the model are respectively summarized in Table 3.1, Table 3.2, and Table 3.3.

Table 3.1 Summary of Input Set Notations

Notation	Description
$\mathcal{R}$	Set of the orders, $r \in \mathcal{R}$
$\mathcal{P}^v$	Set of the candidate nodes for recharging vehicle $v \in \mathcal{V}$, $\mathcal{P}^v \subset \mathcal{S}$
$\mathcal{D}$	Set of destination nodes within the network, $d \in \mathcal{D}$
$\mathcal{S}$	Set of all nodes in the network, including operational, order pickup, recharging, and destination nodes
$\mathcal{V}$	Set of all available vehicles in the network, $v \in \mathcal{V}$
$\mathcal{A}$	Set of arcs connecting nodes $i \in \mathcal{S}$ and $j \in \mathcal{S}$ via vehicle $v \in \mathcal{V}$, $(i, j, v) \in \mathcal{A}$

Table 3.2 Summary of Input Parameter Notations

Parameter	**Description**
C_{ijv}	Cost of shipping orders through the arc $(i,j,v) \in \mathcal{A}$
ω^v	Cost of recharging vehicle $v \in \mathcal{V}$
λ	Cost of transshipping an order from one vehicle to another vehicle
Q_r	Quantity of order $r \in \mathcal{R}$
K_d	Maximum order volume that can be shipped into destination $d \in \mathcal{D}$
U_v	Transportation capacity of vehicle $v \in \mathcal{V}$
$P(r)$	Pickup location associated with order $r \in \mathcal{R}$
$\mathcal{O}^v$	Operational base for vehicle $v \in \mathcal{V}$ to begin its route, $\mathcal{O}^v \in \mathcal{S}$
$\mathcal{O}'^v$	Operational base for vehicle $v \in \mathcal{V}$ to end its route, $\mathcal{O}'^v \in \mathcal{S}$
$a_{P(r)}$	Earliest available time for order $r \in \mathcal{R}$ to be picked up from location $P(r)$
b_r	Latest allowable time for order $r \in \mathcal{R}$ to be delivered to a destination
l_d	Latest allowable delivery time for any order to be delivered to destination $d \in \mathcal{D}$
θ_{ijv}	Time required for traveling from node i to node j via arc $(i,j,v) \in \mathcal{A}$
g^v	Time required for recharging vehicle $v \in \mathcal{V}$
h_{vn}	Time required to transfer orders from vehicle $v \in \mathcal{V}$ to vehicle $n \in \mathcal{V}$
$E^v_{\min}$	Minimum energy reserve required for vehicle $v \in \mathcal{V}$ during its route to ensure safety
$E^v_{\max}$	Maximum energy capacity of vehicle $v \in \mathcal{V}$
M	A positive large number
σ	Small penalty for a later arrival time at a location
$\mathcal{E}^v_{jk}(\mathcal{T}'_{jv})$	Function to calculate energy consumption for vehicle $v \in \mathcal{V}$ departing from node $j \in \mathcal{S}$ to node $k \in \mathcal{S}$ at variable time $\mathcal{T}'_{jv}$

Table 3.3 Summary of Decision Variable Notations

Decision Variable	**Description**
$\mathcal{X}_{ijv}$	Equal to 1 if arc $(i,j,v) \in \mathcal{A}$ is selected to interconnect nodes $i \in \mathcal{S}$ and $j \in \mathcal{S}$ via vehicle $v \in \mathcal{V}$; 0 otherwise
Y_{ijv}^{r}	Equal to 1 if order $r \in \mathcal{R}$ is transited from node i to node j through arc $(i,j,v) \in \mathcal{A}$; 0 otherwise
$\mathcal{Z}_{iv}$	Equal to 1 if vehicle $v \in \mathcal{V}$ is recharged at node $i \in \mathcal{P}^v$; 0 otherwise
$\mathcal{W}_{ijv}$	Equal to 1 if node $i \in \mathcal{S}$ precedes node $j \in \mathcal{S}$ in the route of vehicle $v \in \mathcal{V}$
γ_{ir}^{vn}	Equal to 1 if order $r \in \mathcal{R}$ is transferred from vehicle $v \in \mathcal{V}$ to vehicle $n \in \mathcal{V}$ at node i; 0 otherwise
δ_i	Equal to 1 if at least one order is transshipped from one vehicle to another at node $i \in \mathcal{S}$; 0 otherwise
$\mathcal{T}_{iv}$	Arrival time of vehicle $v \in \mathcal{V}$ at node $i \in \mathcal{S}$
$\mathcal{T}'_{iv}$	Departure time of vehicle $v \in \mathcal{V}$ from node $i \in \mathcal{S}$
E_{iv}	Remaining energy for vehicle $v \in \mathcal{V}$ upon arrival at node $i \in \mathcal{S}$
E'_{iv}	Remaining energy for vehicle $v \in \mathcal{V}$ upon departure from node $i \in \mathcal{S}$

3.5 Mathematical Formulation

In this section, we present the model formulation. The objective function, represented by Equation (3.1), aims to minimize the total operational costs, which include transportation, recharging, and transshipment costs. Fixed costs are not considered in the objective function because the planning horizon is short for the operational decision-making level, and a third-party service provider is assumed to manage the vehicles using existing facility locations. The final term in the objective function incentivizes early arrivals and minimizes slack in the time variables. It also establishes a trade-off between delivery cost and timeliness.

$$\min TC = \sum_{(i,j,v)\in\mathcal{A}} \mathrm{C}_{ijv}\,\mathcal{X}_{ijv} + \sum_{v\in\mathcal{V}}\sum_{i\in\mathcal{P}^v} \omega^v\,\mathcal{Z}_{iv} + \sum_{i\in\mathcal{S}} \lambda\,\delta_i + \sum_{i\in\mathcal{S}}\sum_{v\in\mathcal{V}} \sigma\,\mathcal{T}'_{iv} \tag{3.1}$$

The remainder of this section presents the constraints, grouped according to their focus.

Vehicle Routing Constraints. Constraints (3.2) through (3.4) define the feasible routes and the corresponding arcs within the network. Constraints (3.2) ensures that if a vehicle $v \in \mathcal{V}$ departs from its operational base located at node $i = \mathcal{O}^v$, it travels to one subsequent node $j \in \mathcal{S}$ via the available arc $(i, j, v) \in \mathcal{A}$. Similarly, constraints (3.3) specify that if vehicle $v \in \mathcal{V}$ departs from its operational base, it must return to its corresponding operational base $l = \mathcal{O}'^v$ upon completing its route via one of the available arcs $(j, l, v) \in \mathcal{A}$. Constraints (3.4) enforce that if a vehicle visits an intermediate node $j \in \mathcal{S}$, which is not part of the vehicle's operational bases, it must immediately depart from j via an available arc $(j, i, v) \in \mathcal{A}$.

Constraints (3.5) through (3.7) address sub-tour elimination constraints, enforcing precedence relationships between nodes through linear ordering. To achieve this, a binary variable $\mathcal{W}_{ijv}$ is defined, where $\mathcal{W}_{ijv}$=1 if node $i \in \mathcal{S}$ precedes node $j \in \mathcal{S}$ in the route of vehicle $v \in \mathcal{V}$, otherwise $\mathcal{W}_{ijv}$=0. Constraints (3.5) specify that for an arc $(i, j, v) \in \mathcal{A}$, which neither originates from nor terminates at the operational bases of vehicle $v \in \mathcal{V}$, variable $\mathcal{W}_{ijv}$ is equal to 1 only if node i is connected to node j via vehicle v. Equation (3.6) prohibits the immediate reversal of arcs, ensuring that if vehicle v traverses arc $(i, j, v) \in \mathcal{A}$, it cannot subsequently traverse the reverse arc $(j, i, v) \in \mathcal{A}$. Constraints (3.7) prevent the formation of sub-tours at non-operational nodes, maintaining route continuity.

$$\sum_{(i,j,v)\in\mathcal{A}} \mathcal{X}_{ijv} \leq 1, \quad \forall i = \mathcal{O}^v,\ v \in \mathcal{V} \tag{3.2}$$

$$\sum_{(i,j,v)\in\mathcal{A}} \mathcal{X}_{ijv} = \sum_{(j,l,v)\in\mathcal{A}} \mathcal{X}_{jlv}\,, \quad \forall i = \mathcal{O}^v,\ l = \mathcal{O}'^v,\ v \in \mathcal{V} \tag{3.3}$$

$$\sum_{(i,j,v)\in\mathcal{A}} \mathcal{X}_{ijv} = \sum_{(j,i,v)\in\mathcal{A}} \mathcal{X}_{jiv}\,, \quad \forall j \in \{\mathcal{S} \mid \mathcal{O}^v, \mathcal{O}'^v\},\ v \in \mathcal{V} \tag{3.4}$$

$$\mathcal{X}_{ijv} \leq \mathcal{W}_{ijv}, \quad \forall (i,j,v) \in \mathcal{A}, i \neq \mathcal{O}^v, j \neq \mathcal{O}'^v \tag{3.5}$$

$$\mathcal{W}_{ijv} + \mathcal{W}_{jiv} = 1, \quad \forall (i,j,v), (j,i,v) \in \mathcal{A}, i \neq \mathcal{O}^v, j \neq \mathcal{O}'^v \tag{3.6}$$

$$\mathcal{W}_{ijv} + \mathcal{W}_{jlv} + \mathcal{W}_{liv} \leq 2, \quad \forall (i,j,v), (j,l,v), (l,i,v) \in \mathcal{A}, l \in \mathcal{S}, i,j \neq \mathcal{O}^v, l \neq \mathcal{O}'^v \tag{3.7}$$

Order Delivery Constraints. Here we outline the constraints designed to track each order as it moves through the network. Constraints (3.8) ensure that order $r \in \mathcal{R}$ is picked up from its designated pickup location $\mathrm{P}(r)$ by one of the available vehicles in the network, while equation (3.9) guarantees that the picked-up order r will be delivered to one of the destination nodes. Constraints (3.10) specify that if order r is transshipped to a node that is not a destination, it must be forwarded out of that node. Constraints (3.11) indicate that order r can be transshipped from node i to node j via vehicle v only if arc $(i,j,v) \in \mathcal{A}$ is available in the network.

$$\sum_{(i,j,v) \in \mathcal{A}} \mathcal{Y}_{ijv}^r = 1, \quad \forall r \in \mathcal{R}, i = \mathrm{P}(r) \tag{3.8}$$

$$\sum_{(i,j,v) \in \mathcal{A}} \mathcal{Y}_{ijv}^r = \sum_{(i\prime,j\prime,v) \in \mathcal{A}, j\prime \in \mathcal{D}} \mathcal{Y}_{i\prime j\prime v}^r, \quad \forall r \in \mathcal{R}, i = \mathrm{P}(r) \tag{3.9}$$

$$\sum_{(i,j,v) \in \mathcal{A}} \mathcal{Y}_{ijv}^r = \sum_{(j,i,v) \in \mathcal{A}} \mathcal{Y}_{jiv}^r, \quad \forall r \in \mathcal{R}, j \in \{\mathcal{S}|\mathcal{D}, \mathrm{P(r)}\} \tag{3.10}$$

$$\mathcal{Y}_{ijv}^r \leq \mathcal{X}_{ijv}, \quad \forall (i,j,v) \in \mathcal{A},\ r \in \mathcal{R} \tag{3.11}$$

Capacity Constraints. Constraints (3.12) and (3.13) impose limits to maintain feasibility regarding vehicle and destination capacities. Constraints (3.12) ensure that the total quantity of orders transported through arc $(i,j,v) \in \mathcal{A}$ does not exceed the available capacity of vehicle v. Similarly, constraints (3.13) guarantee that the total quantity of orders delivered to each destination $j \in \mathcal{D}$ remains within the allowable capacity of that destination.

$$\sum_{r\in\mathcal{R}} \mathrm{Q}_r\, \mathcal{Y}^r_{ijv} \le \mathrm{U}_v \mathcal{X}_{ijv}, \quad \forall (i,j,v) \in \mathcal{A} \tag{3.12}$$

$$\sum_{(i,j,v)\in\mathcal{A}} \sum_{r\in\mathcal{R}} \mathrm{Q}_r\, \mathcal{Y}^r_{ijv} \le \mathrm{K}_j, \quad \forall j \in \mathcal{D} \tag{3.13}$$

Transshipment Constraints. The proposed model assumes that orders can be transshipped between vehicles at non-destination nodes. In this context, constraints (3.14) specify that a transshipment occurs at a non-destination node $i \in \mathcal{S}$ if order $r \in \mathcal{R}$ arrives at node i via vehicle $v \in \mathcal{V}$ through arc $(j,i,v) \in \mathcal{A}$ and is subsequently shipped from node $i \in \mathcal{S}$ to node $j' \in \mathcal{S}$ using vehicle $n \in \mathcal{V}$ via arc $(i,j',n) \in \mathcal{A}$. Constraints (3.15) calculate the variable δ_i, which determines whether at least one order is transshipped at node $i \in \mathcal{S}$. Constraints (3.16) ensure that vehicle $n \in \mathcal{V}$ cannot depart from node i, where at least one transshipment is occurring from vehicle $v \in \mathcal{V}$ to vehicle n, until vehicle v has arrived at node i and the orders have been transferred to vehicle n.

$$\sum_{(j,i,v)\in\mathcal{A}} \mathcal{Y}^r_{jiv} + \sum_{(i,j\prime,n)\in\mathcal{A}} \mathcal{Y}^r_{ij\prime n} \le \gamma^{vn}_{ir} + 1, \quad \forall i \in \mathcal{S}|\mathcal{D}, r \in \mathcal{R}, v \in \mathcal{V}, n \in \mathcal{V}, v \neq n \tag{3.14}$$

$$\delta_i \ge \left(\sum_{r\in\mathcal{R}} \sum_{v\in\mathcal{V}} \sum_{n\in\mathcal{V}} \gamma^{vn}_{ir} \right) / \mathrm{M}, \quad \forall i \in \mathcal{S} \tag{3.15}$$

$$T_{iv} + \sum_{r\in\mathcal{R}} h_{vn}\, \gamma^{vn}_{ir} - T'_{in} \le \mathrm{M}(1-\delta_i), \quad \forall i \in \mathcal{S}|\mathcal{D},\ v \in \mathcal{V},\ n \in \mathcal{V},\ v \neq n \tag{3.16}$$

Time Constraints. The constraints (3.17) define the relationship between the arrival and departure time of a vehicle at node $i \in \mathcal{S}$, incorporating the operational activities performed at that node. Each vehicle $v \in \mathcal{V}$ is assumed to be rechargeable at designated recharging stations within the set $\mathcal{P}^v$. That is, they guarantee that vehicle $v \in \mathcal{V}$ departs from node i after its arrival time at node i plus the time required for operational activities. If $i \in \mathcal{P}^v$, operational activities

can include recharging and load or unload during order transshipment operations, otherwise, if $i \notin \mathcal{P}^v$, load or unload can be the only operational activities to be performed at node i. Constraints (3.18) ensure that if node $i \in \mathcal{S}$ is connected to node $j \in \mathcal{S}$ via arc $(i,j,v) \in \mathcal{A}$, vehicle v arrives at node j after departing from node i and traveling for θ_{ijv} hours. Constraints (3.19) and (3.20) impose time window restrictions on each order. Constraints (3.19) ensure that vehicle $v \in \mathcal{V}$ does not pick up order $r \in \mathcal{R}$ before the predefined earliest pickup time for the order's pickup location $\mathrm{P(r)}$, while constraints (3.20) ensure that order r is delivered to destination $i \in \mathcal{D}$ via vehicle v no later than the specified delivery time for order r and the latest delivery time acceptable for the destination i.

$$\begin{cases} \mathcal{T}'_{iv} \geq \mathcal{T}_{iv} + g^v \mathcal{Z}_{iv} + \sum_{r \in \mathcal{R}} h_{vn} \left(\gamma_{ir}^{vn} + \gamma_{ir}^{nv}\right), \quad \forall i \in \mathcal{P}^v, v \in \mathcal{V}, n \in \mathcal{V}, n \neq v \\ \mathcal{T}'_{iv} \geq \mathcal{T}_{iv} + \sum_{r \in \mathcal{R}} h_{vn} \left(\gamma_{ir}^{vn} + \gamma_{ir}^{nv}\right), \quad \forall i \in \mathcal{S} | \mathcal{P}^v, v \in \mathcal{V}, n \in \mathcal{V}, n \neq v \end{cases} \tag{3.17}$$

$$\mathcal{T}'_{iv} + \theta_{ijv} - \mathcal{T}_{jv} \leq \mathrm{M}\left(1 - \mathcal{X}_{ijv}\right), \quad \forall (i,j,v) \in \mathcal{A} \tag{3.18}$$

$$a_{\mathrm{P}(r)} \leq \mathcal{T}'_{iv}, \quad \forall r \in \mathcal{R}, i = \mathrm{P}(r), v \in \mathcal{V} \tag{3.19}$$

$$\mathcal{T}_{iv} \leq min(b_r, l_i) \sum_{(j,i,v) \in \mathcal{A}} \mathcal{Y}_{jiv}^r + \mathrm{M}\left(1 - \sum_{(j,i,v) \in \mathcal{A}} \mathcal{Y}_{jiv}^r\right), \quad \forall i \in \mathcal{D}, v \in \mathcal{V}, r \in \mathcal{R} \tag{3.20}$$

Energy Constraints. Constraints (3.21) and (3.22) ensure energy sufficiency and operational safety for vehicles. Constraints (3.21) guarantee that the remaining energy of vehicle $v \in \mathcal{V}$ upon departing from any node does not exceed its maximum predefined energy capacity, while constraints (3.22) ensure that upon arriving at a node, vehicle v has at least a minimum predefined energy level to maintain safety. Constraints (3.23) specify that each vehicle is fully charged when it starts its trip from its operational base. Constraints (3.24) ensure that vehicle $v \in \mathcal{V}$ can only be recharged at node $i \in \mathcal{P}^v$ if there is an available path to node i via the arc

$(j, i, v) \in \mathcal{A}$. Constraints (3.25) and (3.26) indicate that if vehicle $v \in \mathcal{V}$ is recharged at node $i \in \mathcal{P}^v$, its energy upon departure from node i will be the maximum energy capacity. Constraints (3.7) state that energy level for vehicle $v \in \mathcal{V}$ upon departure from node $i \in \mathcal{S}$ is equal to its energy level upon arrival to node i if recharge does not happen. Constraints (3.8) and (3.9) ensure that if arc $(j, k, v) \in \mathcal{A}$ is available, the remaining energy of vehicle $v \in \mathcal{V}$ upon arriving at node k is equal to its energy upon leaving node j minus the energy consumed during the flight.

$$E'_{iv} \leq \mathrm{E}^{v}_{\max}, \quad \forall i \in \mathcal{S},\ v \in \mathcal{V} \tag{3.1}$$

$$E_{iv} \geq \mathrm{E}^{v}_{\min}, \quad \forall i \in \mathcal{S},\ v \in \mathcal{V} \tag{3.2}$$

$$E'_{iv} \geq \mathrm{E}^{v}_{\max} \sum_{(i,j,v) \in \mathcal{A}} \mathcal{X}_{ijv}, \quad \forall i = \mathcal{O}^v, v \in \mathcal{V} \tag{3.3}$$

$$\mathcal{Z}_{iv} \leq \sum_{(j,i,v) \in \mathcal{A}} X_{jiv}, \quad \forall i \in \mathcal{P}^v, v \in \mathcal{V} \tag{3.4}$$

$$E'_{iv} - E_{iv} \leq \mathrm{M}\mathcal{Z}_{iv}, \quad \forall i \in \mathcal{P}^v, v \in \mathcal{V} \tag{3.5}$$

$$E'_{iv} \geq \mathrm{E}^{v}_{max}\mathcal{Z}_{iv}, \quad \forall i \in \mathcal{P}^v, v \in \mathcal{V} \tag{3.6}$$

$$E'_{iv} - E_{iv} \geq 0, \quad \forall i \in \mathcal{S}, v \in \mathcal{V} \tag{3.7}$$

$$E'_{jv} - \mathcal{E}^{v}_{jk}\left(\mathcal{T}'_{jv}\right) \leq E_{kv} + \mathrm{M}\left(1 - \mathcal{X}_{jkv}\right), \quad \forall v \in \mathcal{V}, (j, k, v) \in \mathcal{A} \tag{3.8}$$

$$E'_{jv} - \mathcal{E}^{v}_{jk}\left(\mathcal{T}'_{jv}\right) \geq E_{kv} - \mathrm{M}\left(1 - \mathcal{X}_{jkv}\right), \quad \forall v \in \mathcal{V}, (j, k, v) \in \mathcal{A} \tag{3.9}$$

The next chapter presents the case study used in this research to verify and validate the proposed model's performance.

Chapter 4 Chapter 4 Shield Illinois Case Study Data

During the global COVID-19 pandemic, Shield Illinois emerged as a pioneering initiative led by the University of Illinois System. Its mission was to deploy an innovative saliva-based COVID-19 test to serve schools, universities, community centers, and the public across Illinois. We apply our proposed model to a case study based on operations from Shield, with pickup site locations including schools, colleges, and universities where COVID-19 tests were conducted. The samples collected from these pickup sites were transported to diagnostic labs, treated as identical but capacitated destinations. This chapter provides detailed information about Shield Illinois, their operations, and the processes involved in building the case study. This case study serves as the foundation for the input data used in verifying and validating the proposed model, as well as for deriving valuable insights in the next chapter.

Figure 4.1 Saliva-based covid Shield COVID-19 test

4.1 Shield Illinois: An Overview

Shield Illinois (referred to as “Shield” for brevity) is the University of Illinois System’s initiative to make the innovative saliva-based Shield COVID-19 test (see Figure 4.1) available to 1,779 K-12 schools, 57 universities and community colleges, and the public across the state of

Illinois with 77 community-based sites (see Figure 4.2). This initiative, created in response to an urgent public health crisis, successfully delivered over seven million tests between July 2020 and June 2023. With a network of 13 diagnostic laboratories and a logistics system spanning a 400-by-200-mile area, Shield Illinois maintained an impressive 16-hour average turnaround time, processing between 10,000 and 14,000 samples daily during peak periods. This efficiency far outpaced other testing programs, which often required two to three days to deliver results. While all testing centers were located in Illinois, the Shield T3 program extended operations to Kentucky and Wisconsin, utilizing existing labs to meet the rising demand during critical periods.

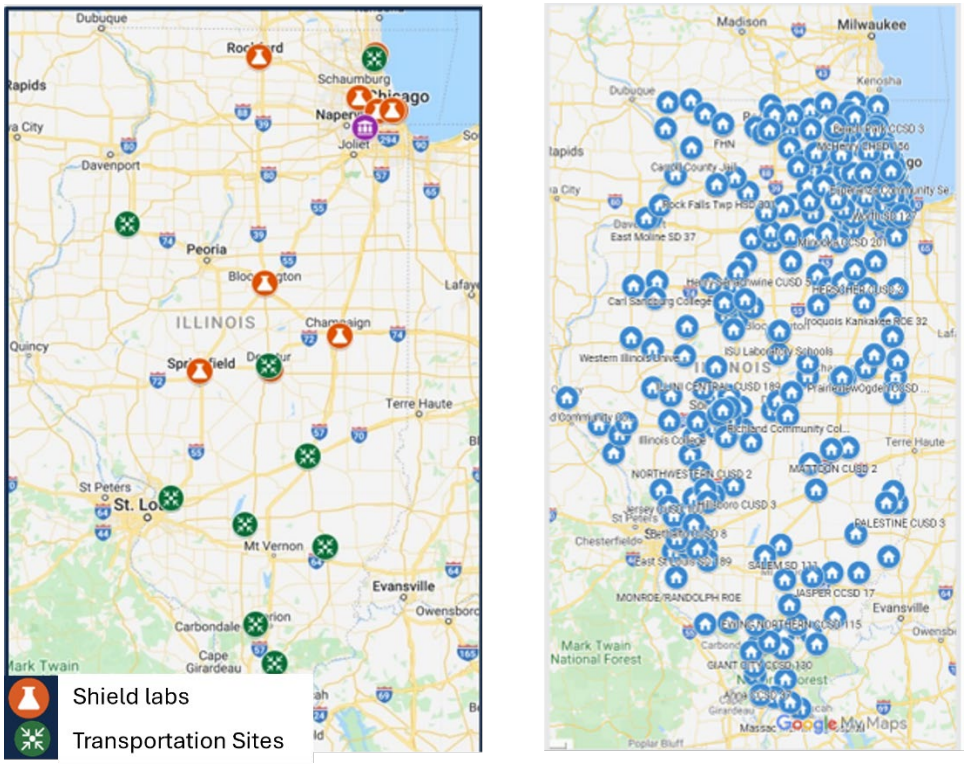

Figure 4.2 Statewide logistics network of Shield; left map shows the labs and transportation sites; right map shows all test site locations.

It was formed urgently during the global pandemic to save lives in Illinois. With 13 labs networked together and a 400-by-200-mile logistics system, including the Chicago metropolitan, Shield ran over seven million total tests between July 2020 and June 2023. Shield maintained 16-hour average turnaround times even during peak periods, compared to other testing programs that delivered in two to three days. Each lab processed between 10,000 and 14,000 samples daily during peak periods of the pandemic.

4.1.1 The Testing Process

The saliva-based testing process began with specimen collection at over 2,000 testing centers across Illinois. Saliva samples, referred to as "specimens", were collected in test tubes and transported to diagnostic labs for analysis. Upon arrival at the labs, the specimens underwent sample preparation, as saliva could not be directly tested using PCR methods. This preparation involved heating the saliva and combining it with a buffer and detergent to create "samples," which were then transferred to 96-well plates. These plates, referred to as "Plate 96", each contained one sample per well and were loaded into PCR machines for testing. The test results were subsequently delivered to individuals, enabling timely health interventions.

4.1.2 Transport and Tracking

Shield's transport and tracking system ensured efficient specimen movement from collection sites to labs. At the core of this system was the "manifest", a digital tracking mechanism used to monitor specimens from each testing center. A manifest was created when testing began at a location and closed at the end of the day. The size of a manifest varied depending on testing volume, ranging from a single specimen to large batches. Multiple manifests could also originate from the same location on a given day.

Specimens were first transported to a centralized depot in Darien, IL, often referred to as "Lab 12". At the depot, specimens were manually sorted and assigned to specific labs based on workload and processing efficiency. This sorting process ensured balanced workloads across Shield's 13 labs and minimized delays. Some testing centers dispatched specimens at specific times during the day, while others waited until testing concluded.

The depot played a crucial role in load balancing and ensuring quicker turnaround times. Once sorted, specimens were sent to the designated labs for processing, often bypassing direct routes to optimize logistics.

4.1.3 Lab Operations and Network Capacity

Shield Illinois operated a network of 13 diagnostic labs, with facilities distributed across Illinois and additional locations in Kentucky and Wisconsin to manage peak volumes. The labs varied in size, capacity, and resources, including the number of technicians and available equipment. For instance, the lab at Loyola University utilized existing infrastructure to expedite setup, while Shield T3 labs in Kentucky and Wisconsin supported overflow during periods of increased demand.

Each lab processed between 10,000 and 14,000 samples daily during peak periods, ensuring rapid turnaround times even under significant pressure. The labs' ability to maintain consistent performance was critical to Shield's success and exemplified the program's adaptability and efficiency.

4.1.4 Serving the Community

Shield Illinois provided testing services to a wide range of institutions, including K-12 schools, colleges, universities, and community centers. Community center selection was guided by the Social Vulnerability Index (SVI), ensuring equitable access to testing for underserved

populations. Schools identified under Tiers 1 and 2 of evidence-based funding criteria received free testing, further emphasizing the program's commitment to equity.

4.1.5 Impact and Legacy

Shield Illinois demonstrated a highly effective response to a global health crisis, setting a benchmark for large-scale, rapid diagnostic testing programs. By combining innovative saliva-based testing with a streamlined logistics network, the initiative achieved remarkable milestones, including same-day delivery of specimens to labs and consistent 16-hour turnaround times. The program's efficiency, scalability, and commitment to public health made it a critical tool in combating the pandemic, saving countless lives, and establishing a model for future public health initiatives.

4.2 Data Sets and Data Processing

To support the development and validation of the proposed model, we utilized a variety of datasets that capture different aspects of Shield Illinois's COVID-19 testing operations. These datasets, encompassing millions of records, provided insights into the logistical, operational, and testing processes across the initiative. Each dataset brought unique attributes essential for analyzing and modeling the intricate system. The following outlines the datasets, their characteristics, and the steps taken to process and prepare the data for use.

The data included critical components such as specimen and sample information, plate processing details, equipment data, testing center records, and manifests tracking the transportation of specimens. Specimen and sample datasets were among the largest, documenting the lifecycle of specimens from collection at testing centers to results processing in labs. Key attributes included timestamps marking collection, transport, and result generation, as well as IDs linking specimens to samples. To clarify relationships, we ensured that each specimen

corresponded to a single sample, resolving confusion arising from the interchangeable use of these terms in operational data.

Plate and equipment datasets tracked the technical aspects of sample processing. The plate data captured the movement of samples through testing equipment, recording attributes such as plate IDs, associated technician IDs, and timestamps. Meanwhile, the equipment dataset provided information about the machines used in labs; though some fields, such as equipment types, had missing or inconsistent entries that required careful examination and resolution.

Testing center and manifest data provided a spatial and temporal view of operations. Testing centers were identified by their SHIELD IDs, geocodes, and operational details. The manifest data tracked specimens from testing sites to labs, offering insights into transportation times, routes, and load balancing. Some manifests indicated specimens were routed through a centralized depot, where sorting occurred to manage lab workloads efficiently.

Additional datasets included records of *specimen rejection*, providing reasons such as canceled orders or failure to meet collection standards. *Depot rerouting data* detailed the manual sorting of specimens, ensuring timely delivery to appropriate labs. Account and opportunity data from Shield's CRM offered contextual information about testing site categories, geolocations, and operational settings.

Processing and cleaning this data involved multiple steps to ensure accuracy and reliability. Missing data, particularly in fields such as equipment type and timestamps, was addressed by cross-referencing other datasets or excluding incomplete records where necessary. Location names were standardized to resolve discrepancies and enable matching across datasets, and unique SHIELD IDs and geocodes were assigned to ensure a consistent spatial

representation of the network. Relationships between key entities, such as specimens, samples, and plates, were validated to ensure logical consistency.

Timestamps posed particular challenges, as multiple datasets recorded different stages of processing. These were carefully aligned and verified to maintain a coherent sequence of events, such as manifest creation, transportation, and lab processing. Ambiguities in the data, such as plates that appeared in processing records but not in scanning datasets, were flagged for further investigation and resolution.

The processed datasets were then prepared as inputs for the proposed model. Cleaned and integrated tables were created, combining attributes such as testing site locations, specimen volumes, lab capacities, and turnaround times. Operational constraints, including lab processing limits and testing schedules, were defined from the data to align with real-world practices. The final datasets were cross-validated against business rules and operational knowledge from Shield Illinois to ensure their robustness and suitability for modeling.

4.3 Case Study and Parameter Calibration

For this study, we focus on one of the busiest labs and its associated testing sites—over 60 testing locations—in the southwest rural region of the state (see Figure 4.3). The entire case study region includes three Voronoi regions corresponding to three weather stations. During the Omicron wave, spanning January 1, 2022, to June 30, 2022, these locations processed between 10,000 and 14,000 samples per lab per day during peak periods. The study area covers approximately 2,022 square miles, including 40 order locations (testing sites) and one laboratory as the destination for all orders. The maximum distance between a pickup location and the lab is 125 miles. Our case study includes the pickup orders on February 9, 2022.

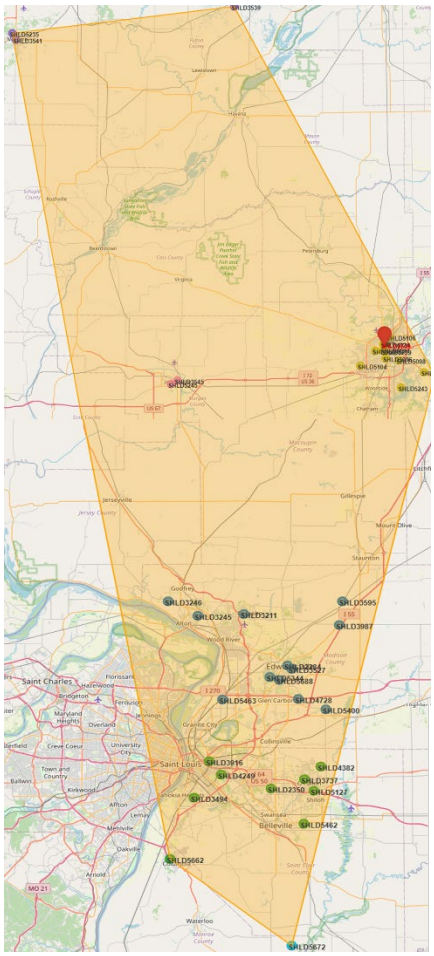

Figure 4.3 Service region selected for the case study- southwest area of Illinois State

4.3.1 Shield Delivery System

The Shield delivery system operated on a point-to-point model, relying on ground transport (SUVs and cars) without employing routing optimization strategies. Test samples were transported directly from testing sites to the lab throughout the day. This section analyzes the delivery statistics to describe trends and potential inefficiencies.

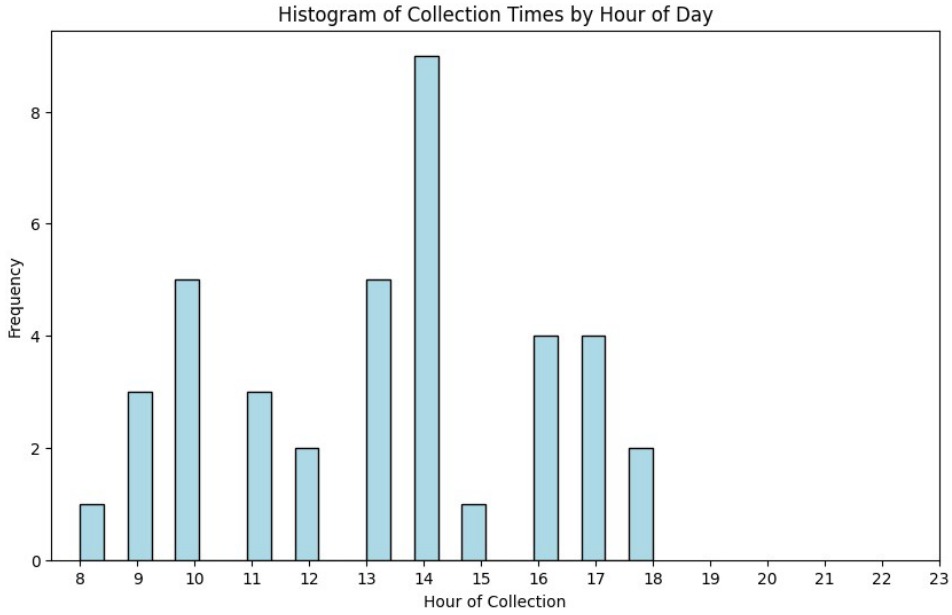

Figure 4.4 Histogram of collection times by hour of day

Figure 4.4 illustrates the distribution of collection times from testing sites in the case study, when 39 deliveries were made to the lab. The data reveals that the highest frequency of collections occurred at 2 PM, with approximately nine collections recorded during this hour. This indicates that most testing sites prepared and dispatched their samples between early and mid-afternoon. Activity gradually increased throughout the morning, starting at 8 AM, before peaking in the early afternoon. After 2 PM, the frequency of collections declined, remaining steady between 3 PM and 5 PM, before dropping significantly in the evening. By 6 PM, collection activity was minimal, highlighting reduced operations in the late afternoon and evening hours.

This pattern suggests a concentration of collections during specific periods, particularly in the mid-afternoon. Such clustering likely creates bottlenecks in transportation and lab processing during peak hours, as a large number of samples are transported and processed within

a short time frame. Conversely, the low activity observed in the early morning and evening hours may result in underutilized transportation resources, leaving room for operational inefficiencies.

Integrating drones into the delivery system could balance workloads by enabling more frequent and flexible collections, reducing peak-hour congestion, and improving transportation efficiency. Drones can operate during off-peak hours, addressing reduced evening activity and resource limitations, while enhancing speed and reliability in sample delivery.

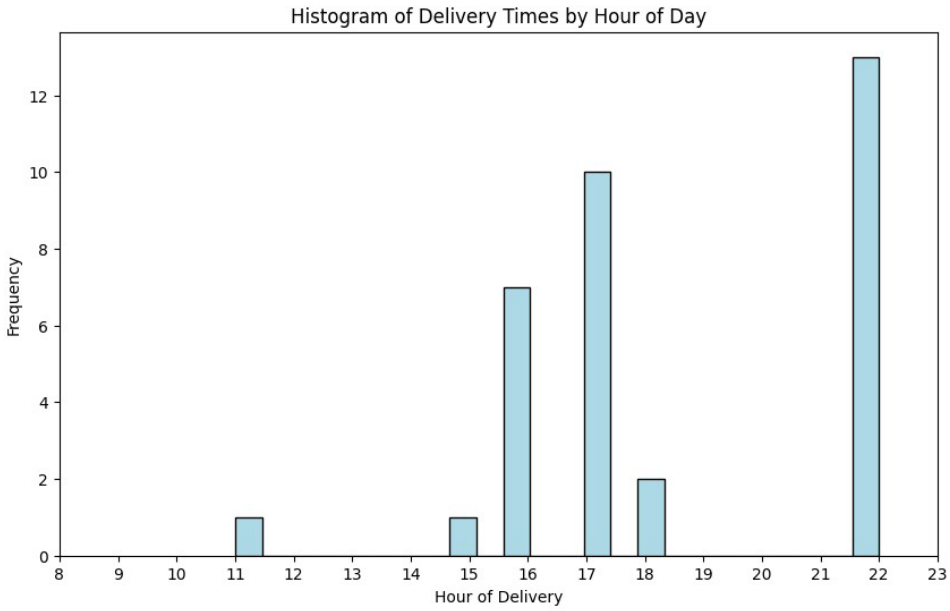

Figure 4.5 Histogram of Delivery Times by Hour of Day

Figure 4.5 illustrates the distribution of delivery times to the lab in the case study. The delivery times ranged from the earliest recorded time of 11:31 AM on February 9 to the latest delivery time of 6:20 PM on February 10, highlighting that some deliveries extended into the next day. The histogram shows that same-day deliveries were heavily concentrated in the late afternoon and evening, with a significant peak at 10 PM, emphasizing delays in the delivery process.

The late delivery patterns and the presence of next-day deliveries reveal inefficiencies in the current delivery system. Specifically, 13% of orders and 11% of samples were delivered the following day, indicating a gap in synchronizing collection schedules with transportation logistics. Moreover, the average ready-to-delivery time—the time elapsed between when a delivery was ready for pickup and its arrival at the lab—was approximately 7.57 hours, further pointing to a lag in the system.

When combined with the earlier collection time analysis, this data suggests a mismatch between the times samples are collected and when they are transported, leading to prolonged delivery times. These delays may contribute to bottlenecks at the lab, reducing processing efficiency and potentially affecting the timeliness of test results. Addressing these synchronization issues could significantly improve overall efficiency and reduce delivery delays.

Figure 4.6 and Figure 4.7 depict the distribution of ready-to-delivery times for orders (deliveries) and individual samples, respectively. These histograms provide insights into the delivery performance and delays within the current logistics system.

In Figure 4.6, the ready-to-delivery times for orders reveal that the majority (over 70%) are delivered within 10 hours. Specific thresholds highlighted in the figure show that 7.69% of orders are delivered within 1 hour, 46.15% within 5 hours, and 87.18% within 15 hours. A small percentage of orders exceed the 15-hour threshold, pointing to inefficiencies in the delivery process. These delays suggest that a significant portion of deliveries falls short of rapid fulfillment, highlighting room for improvement in response times.

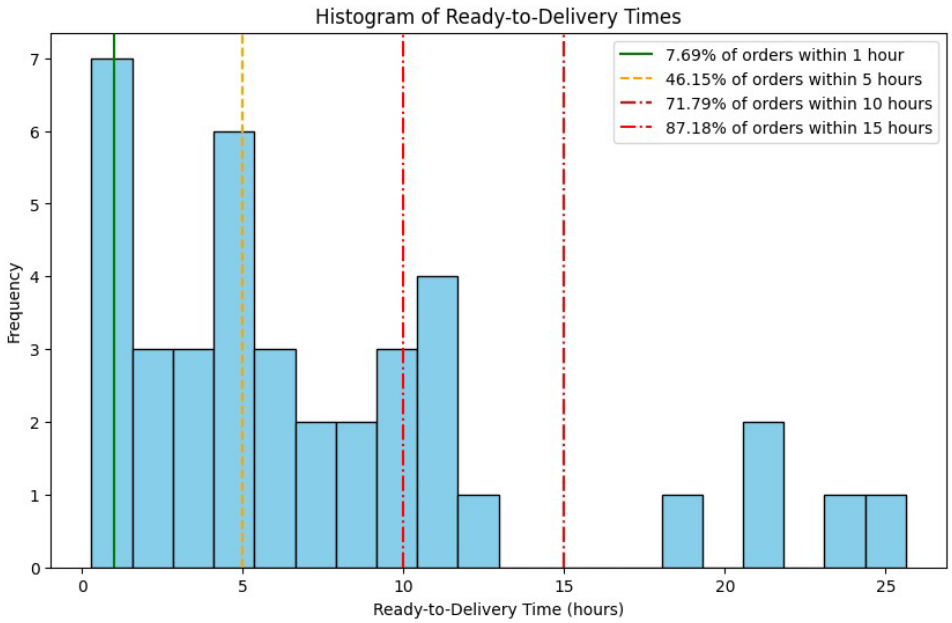

Figure 4.6 Histogram of Ready-to-Delivery Times for Orders. The vertical lines indicate thresholds for delivery times with associated cumulative percentages.

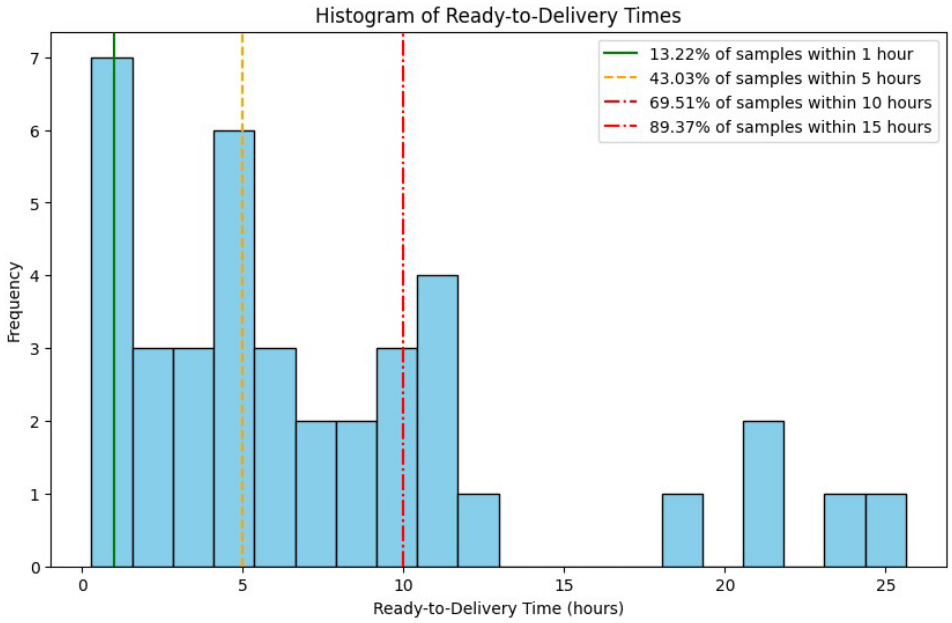

Figure 4.7 Histogram of Ready-to-Delivery Times for Samples. The vertical lines indicate thresholds for delivery times with associated cumulative percentages.

Similarly, Figure 4.7 shows the ready-to-delivery times for individual samples, with delivery times heavily concentrated within the 10-hour range. The breakdown indicates that 13.22% of samples are delivered within 1 hour, 43.03% within 5 hours, 69.51% within 10 hours, and 89.37% within 15 hours. Like the orders, a smaller portion of samples experience delivery delays beyond 15 hours, reflecting limitations in the current system's ability to provide timely deliveries.

The total routing cost for these deliveries was calculated to be $54,307.96, based on a marginal cost of $29 per mile for ground transportation. This analysis underscores the constraints of the existing point-to-point delivery model, which struggles with both response time and cost efficiency.

These findings again highlight the potential benefits of integrating drones into the logistics network. By enabling faster and more flexible deliveries, drones could reduce delivery times, particularly for urgent orders and samples, while also offering opportunities to optimize routing costs and improve overall system efficiency. This analysis sets the stage for exploring how drone integration could address the identified limitations and enhance operational performance.

We completed the case study data by adding car arcs between every pair of nodes and drone arcs between every pair of nodes within the same Voronoi region, along with a few drone arcs connecting different Voronoi regions. Using the MRCC Climate Database (https://mrcc.purdue.edu/CLIMATE/welcome.jsp), we collected weather information and created time-series data of energy consumption for every hour of the day, corresponding to the planning horizon of the case study. A linear regression model was then fitted to estimate the input function

required for the optimization model (refer to Sections 3.3 and 3.5 for more details). Figure 4.8 shows one example for the fitted function on an interregional arc.

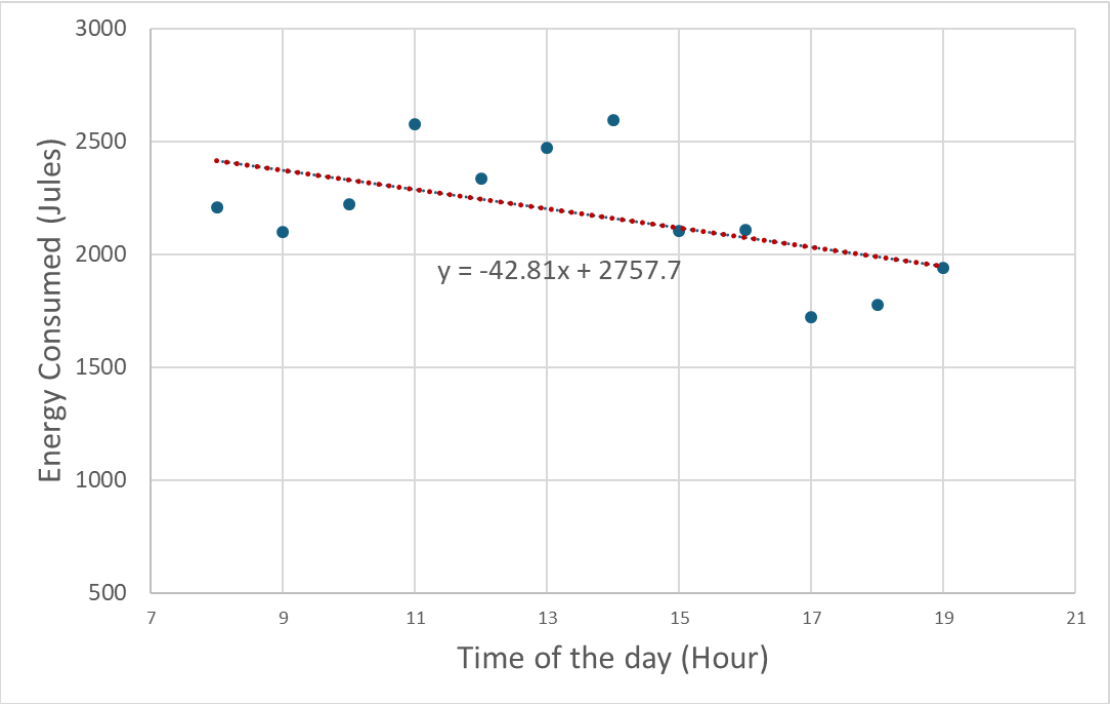

Figure 4.8 Time-Depended Energy Consumption on an Interregional Arc.

These estimated functions (with their slopes and intercepts) are added to the case study data as input for the optimization model. The next section explores various scenarios to evaluate the potential benefits of integrating drones into such a delivery system.

Chapter 5 Chapter 5 Computational Experiments

In this chapter, we evaluate the effectiveness of the proposed optimization model introduced in Chapter 3 by applying it to the case study detailed in Chapter 4. This evaluation is conducted from both operational and managerial perspectives to ensure a comprehensive analysis of its practical applications and implications.

The primary objectives of this chapter are twofold. First, we aim to provide decision-makers with actionable insights into the trade-offs between key performance metrics, including the total cost of delivery routes and adherence to delivery time schedules. Second, we explore broader managerial considerations, such as the environmental impact in terms of emissions, the utilization efficiency of different transportation modes, and the computational runtime of the solver under varying scenarios and considerations.

Furthermore, the chapter delves into the strategic benefits of integrating drones into a multi-modal transportation network. We discuss how leveraging drones, alongside traditional ground vehicles, can enhance the flexibility, responsiveness, and sustainability of delivery systems. Additionally, we emphasize the advantages of using an optimization model for coordinated routing and scheduling, demonstrating its potential to improve operational efficiency and support data-driven decision-making. Finally, the chapter concludes with a critical discussion of the limitations inherent in the model.

5.1 Defining the Experimental Scenarios

Our experiments are categorized into three main groups to evaluate the performance and adaptability of the proposed optimization model under various conditions. These categories and their corresponding scenarios are described as follows:

(1) Ground Vehicle-Only System (GV): This category evaluates the model's performance for a system consisting solely of ground vehicles, with no drones included in the network. Configurations in this category involved either one or two cars, each with a large capacity considered effectively unlimited within the scope of the loads required for this case study. These scenarios provide valuable insights into the operational efficiency, cost-effectiveness, and scheduling performance of a ground-based transportation system, serving as a base case for understanding the capabilities and limitations of traditional logistics approaches.

Scenarios:

- Scenario 1: Single car for the entire case study region.
- Scenario 2: Two cars for the entire case study region.

(2) Weather-Aware Multi-Modal Network (WAMN): This category incorporates drones into the logistics network alongside ground vehicles, creating a multi-modal transportation system. Configurations tested included one car and either three drones (one drone per Voronoi region) or six drones (two drones per Voronoi region). All drones are assumed to be identical small quadcopters with a maximum payload capacity of eight pounds. The analysis in this category focuses on how weather conditions influence energy consumption, operational feasibility, and delivery performance. Explicitly accounting for weather-dependent energy consumption highlights the potential of weather-aware multi-modal systems to improve cost efficiency and service levels.

Scenarios:

- Scenario 3: One car with three drones (one drone per Voronoi region).
- Scenario 5: One car with six drones (two drones per Voronoi region).

(3) Non-Weather-Aware Multi-Modal Network (NWAMN): This category evaluates the impact of ignoring weather conditions in logistics planning. We compared the results with the benchmark model proposed by Enayati et al. (2023), which assumes that drones have a fixed maximum flight range and require recharging after reaching their predefined operational limit, with no weather-related energy consumption considerations. By contrasting the results from the NWAMN scenarios with those from the WAMN category, we assessed the influence of weather-aware modeling on decision variables, such as routing and scheduling, as well as on the overall objective function (i.e., total cost). This comparison underscores the importance of incorporating weather constraints into the design of robust and efficient logistics networks.

Scenarios:

- Scenario 4: One car with three drones (one drone per Voronoi region).
- Scenario 6: One car with six drones (two drones per Voronoi region).

To implement this category of experiments, we substitute the energy consumption constraints (3.21) through (3.29) with the following modified set of constraints:

$$\Delta_{iv} = 0, \quad \forall v \in \mathcal{V}, i = \mathcal{O}^v \tag{5.10}$$

$$\Delta_{iv} \leq \Omega^v * (1 - \mathcal{Z}_{iv}), \quad \forall v \in \mathcal{V}, i \in \mathcal{P}^v \tag{5.11}$$

$$\Delta_{jv} + \left(1 - \mathcal{X}_{ijv} - \mathcal{Z}_{iv}\right) * \Omega^v \geq \Delta_{iv} + \mathcal{X}_{ijv} * L_{ijv}, \quad \forall (i,j,v) \in \mathcal{A}, i \in \mathcal{P}^v \tag{5.12}$$

$$\Delta_{iv} + \mathcal{X}_{ijv} * L_{ijv} \leq \Omega^v \quad \forall (i,j,v) \in \mathcal{A} \tag{5.13}$$

In this formulation, the variable Δ_{iv} represents the cumulative distance traveled by vehicle $v \in \mathcal{V}$ upon arriving at node $i \in \mathcal{S}$. The parameters Ω^v and L_{ijv} denote the maximum distance range that vehicle $v \in \mathcal{V}$ can travel without recharging and the distance between nodes $i \in \mathcal{S}$ and $j \in \mathcal{S}$ via vehicle $v \in \mathcal{V}$, respectively. Constraints (5.1)

ensure that the cumulative traveled distance Δ_{iv} is initialized to zero for each vehicle $v \in \mathcal{V}$ at its starting operational base. Constraints (5.2) enforce that the cumulative traveled distance by vehicle $v \in \mathcal{V}$ does not exceed the vehicle's maximum distance range Ω^v, requiring the vehicle to recharge if necessary. Constraints (5.3) calculate the cumulative distance traveled by vehicle $v \in \mathcal{V}$ on its route on the arc $(i, j, v) \in \mathcal{A}$ while resetting it in case the vehicle v is recharged at node $i \in \mathcal{P}^v$. Constraints (5.4) restrict the cumulative traveled distance to remain within the vehicle's maximum range Ω^v, ensuring operational feasibility for each arc $(i, j, v) \in \mathcal{A}$.

Table 5.1, presented below, summarizes the experimental categories and their corresponding scenarios described above. It details the specific configurations of vehicles and drones used in each scenario, including the allocation of drones across three Voronoi regions in the case study, to support the comparative analysis of the proposed logistics strategies.

Table 5.1 Mapping Experiment Categories to Scenarios

Category	**Scenario**	**Configuration**
Ground Vehicle-Only System (GV)	Scenario 1	1 car
	Scenario 2	2 cars
Weather-Aware Multi-Modal Network (WAMN)	Scenario 3	1 car with 3 drones
	Scenario 5	1 car with 6 drones
Non-Weather-Aware Multi-Modal Network (NWAMN)	Scenario 4	1 car with 3 drones
	Scenario 6	1 car with 6 drones

We assume delivery costs of $29 per mile for cars and $20 per mile for drones. Additionally, all orders are assumed to be ready for pickup at 8:00 AM and are required to be delivered no later than 3:00 PM. We assumed the cost of recharging a drone to be $1 per recharge and the cost of transshipment to be $1 per location where transshipment occurs, regardless of the number of orders transferred between vehicles. We evaluated the performance of all scenarios within each category using key metrics, including total cost, the latest delivery time of orders, the total distance traveled by each transportation mode, emissions, and the solver runtime required to find optimal solutions. For each scenario, the model was executed across multiple operational bases, and the best-case results were reported.

All numerical experiments were conducted on a high-performance system featuring a 16-core CPU running at 3.4 GHz with 94 GB of RAM. The optimization model was implemented and solved using the Gurobi solver within the Python programming environment.

5.2 Numerical Results

In this section, we present the optimal solution configuration and analyze the performance measures for the six scenarios outlined in Table 5.1. A detailed comparison of these scenarios highlights their relative strengths, weaknesses, and overall effectiveness in meeting the operational objectives. The analysis focuses on evaluating key metrics such as cost efficiency, delivery timeliness, and environmental impact, while examining how the inclusion of drones and weather considerations influences performance.

5.2.1 Solution Configuration of Ground Vehicle-Only Scenarios (GV Category)

In the first two scenarios, categorized under Ground Vehicle-Only (GV), only cars are available in the network for transportation. Scenario 1 assumes a single car handles all deliveries within the service region. The optimization model in this scenario aims to minimize total

transportation and recharging costs while adhering to all constraints outlined in Section 3.5, with the exception of the transshipment constraints (3.14 through 3.16). Since only one vehicle is responsible for all deliveries, transshipment variables are excluded from the model.

The results for Scenario 1 are illustrated in Figure 5.1, which shows the optimal routes determined by the model. The car begins its route at the furthest node from the final destination, efficiently servicing intermediate nodes before concluding the trip at the lab. This routing strategy minimizes total distance traveled while ensuring timely delivery of supplies.

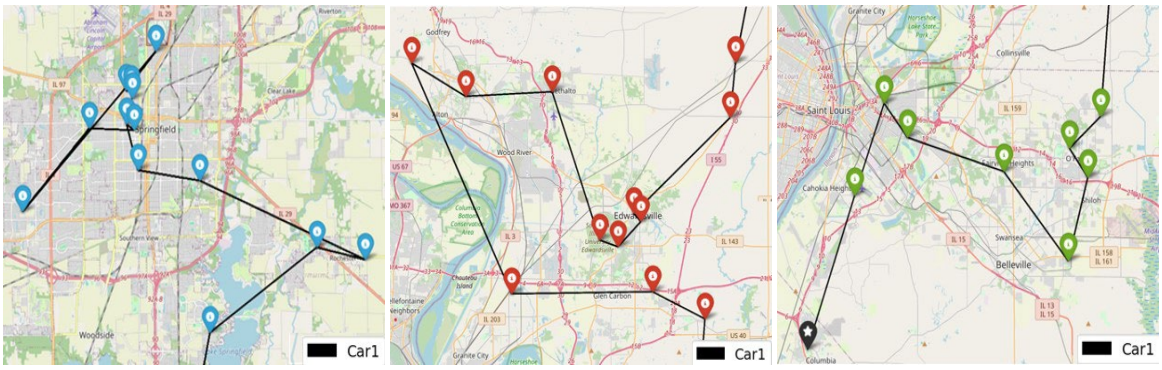

Figure 5.1 Optimal Routes in the Network with One Available Car (Scenario 1). The left, middle, and right maps illustrate the optimal routes within Voronoi regions 1, 2, and 3, respectively.

Scenario 2 expands upon the configuration of Scenario 1 by introducing a second car into the network, allowing for a more detailed analysis of how additional vehicles impact cost, delivery time, and overall operational efficiency. This scenario facilitates a comparison between single-vehicle and multi-vehicle logistics strategies, offering insights into the trade-offs associated with increased fleet size. To accommodate the presence of a second vehicle, the optimization model was updated to include transshipment variables in both the objective function and the relevant constraints, enabling coordination between the two cars. The optimal solution

for Scenario 2 is illustrated in Figure 5.2, where the routes for the two cars are represented by red and blue paths. In this optimal configuration, the second car initiates its route from the farthest node within Voronoi Region 1 (VR 1) and concludes its trip at the destination node, the lab. This routing strategy ensures an efficient division of labor between the two vehicles, reducing total delivery time and optimizing resource utilization while adhering to the system's constraints. The inclusion of a second car also highlights the operational benefits of distributed routing and increased capacity within the network.

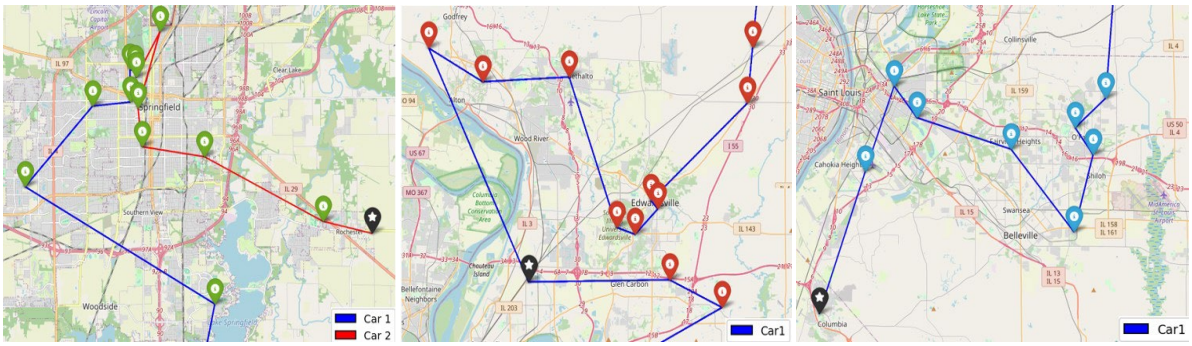

Figure 5.2 Optimal Routes in the Network with Two Available Cars (Scenario 2). The left, middle, and right maps illustrate the optimal routes within Voronoi regions 1, 2, and 3, respectively.

It is worth noting that a scenario involving a third car starting in Voronoi Region 2 (VR 2), resulting in a total of three cars, was also tested but showed that the optimal solution required no more than two cars. This was primarily due to the significant distance between VRs 1 and 2 and VR 3, where the final destination (lab) is located, which made additional cars in distant regions cost-inefficient. Additionally, the high capacity of the cars allowed them to handle all orders without requiring transshipment.

Similar to Figure 5.2, the optimal solution for the other cases of three or more cars consistently deployed the second car exclusively within VR 3, the region containing the final destination. Adding cars to other regions increased transportation costs without improving performance. As a result, scenarios with more than two cars were excluded from further analysis due to their lack of cost-effectiveness.

5.2.2 Solution Configuration of Multi-Modal Coordinated Scenarios (WAMN and NWAMN Categories)

In this subsection, we integrate drones into the network and analyze Scenarios 3 through 6. The Weather-Aware Multi-Modal Network (WAMN) scenarios include Scenarios 3 and 5, which represent the direct implementation of the proposed model described in Section 3.5. To evaluate the impact of weather conditions on the network's performance, we modified the model as discussed in Section 5.1, comparing it against a benchmark model. The results for these comparisons are reported under Scenarios 4 and 6.

In Scenarios 3 and 4, one drone was deployed per Voronoi region. Scenario 4 mirrors Scenario 3 but does not account for weather conditions, instead assuming a fixed flight range regardless of environmental factors. The results for these scenarios are illustrated in Figure 5.3 and Figure 5.4, respectively.

As shown in Figure 5.3, the optimal solution for Scenario 3 utilized all drones across the regions. This widespread usage of drones was driven by their lower operational cost and the favorable impact of weather conditions on energy consumption. Accounting for weather allowed drones to operate more efficiently, as favorable conditions reduced energy usage and extended their effective range.

In contrast, the middle map in Figure 5.4 highlights a limitation in the non-weather-aware model used in Scenario 4. It shows that the drone in Voronoi Region 2 (VR 2) could not operate in the optimal solution due to the fixed flight range assumption. This restriction demonstrates the critical role of weather-aware modeling in enabling drones to adapt to varying environmental conditions. When weather is considered, drones benefit from extended operational ranges under favorable conditions, improving their utility and cost-effectiveness. Without this consideration, the fixed range is strictly proportional to the distance traveled, which significantly limits drone usage in regions requiring longer travel distances. This comparison underscores the importance of incorporating weather-dependent energy consumption into the optimization model, as it not only enhances drone operations but also leads to more efficient and cost-effective solutions for the network.

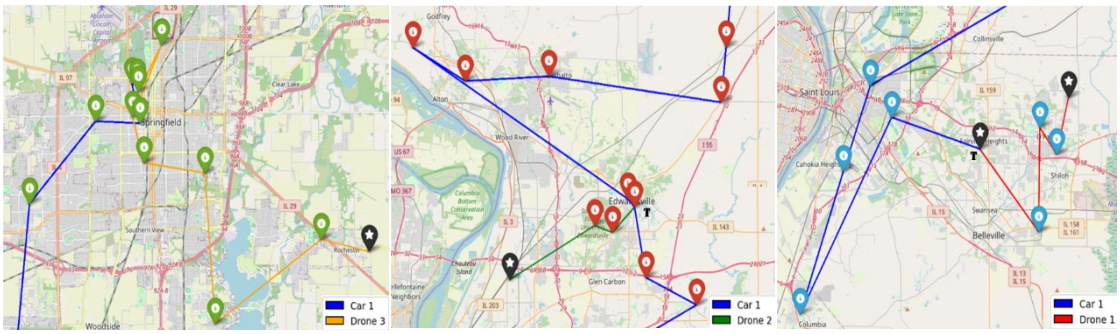

Figure 5.3 Optimal Routes for the Weather-Aware Network with One Car and Three Drones (Scenario 3). The maps on the left, middle, and right depict the optimal routes within Voronoi Regions 1, 2, and 3, respectively. Each drone is assigned to a distinct region, and nodes marked with 'T' indicate transshipment points where test kits are transferred from a drone to the car.

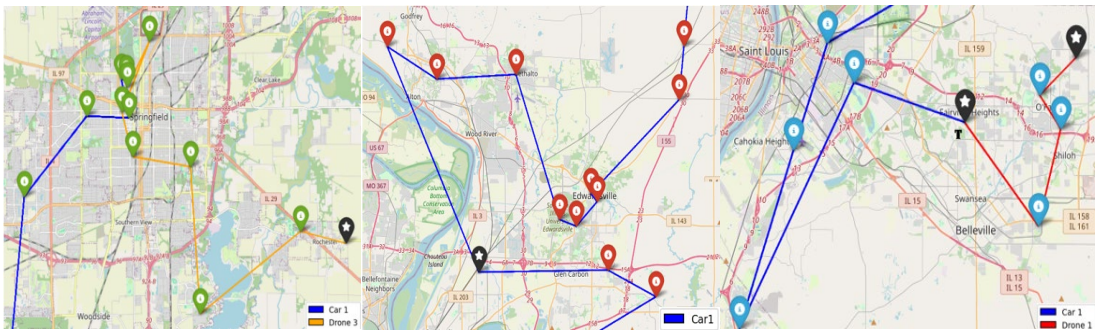

Figure 5.4 Optimal Routes for the Non-Weather-Aware Network with One Car and Three Drones (Scenario 4). The maps on the left, middle, and right depict the optimal routes within Voronoi Regions 1, 2, and 3, respectively. Each drone is assigned to a distinct region, and nodes marked with 'T' indicate transshipment points where test kits are transferred from a drone to the car.

Finally, Figure 5.5and Figure 5.6 depict the routing solutions for Scenarios 5 and 6, revealing that the delivery routes and mode utilization are similar between these two scenarios, with only minor differences. One noticeable distinction lies in the drone route within Voronoi Region (VR) 3, where the order of traversal through three identical locations differs slightly. This difference reflects how the two scenarios handle timing and energy optimization for drone operations. Since the lab is located in VR 1, packages must be transported from VR 3 through VR 2 to reach VR 1. A deeper analysis indicates that Scenario 5 incorporates weather-aware considerations for drone energy consumption, factoring in the anticipated weather conditions at future locations a drone is scheduled to visit. Specifically, the prediction model for energy consumption—dependent on the arrival time at a location—encourages the drone to delay its arrival slightly within VRs 2 and 3. This delay allows the drone to take advantage of lower energy consumption associated with more favorable weather conditions later in the day. This adjustment highlights the sophistication of the weather-aware model, which strives for energy efficiency. However, this approach is only realistic if the energy consumption predictions, based on the expected weather conditions, are accurate at the time of planning. Otherwise, this reliance

on predictive inputs could be seen as a limitation of the model. The model assumes that weather-related predictions are precise and uses them as a function of arrival time to calculate energy consumption for traveling along arcs. Section 5.3 delves deeper into this modeling limitation, providing additional examples and discussing possible implications.

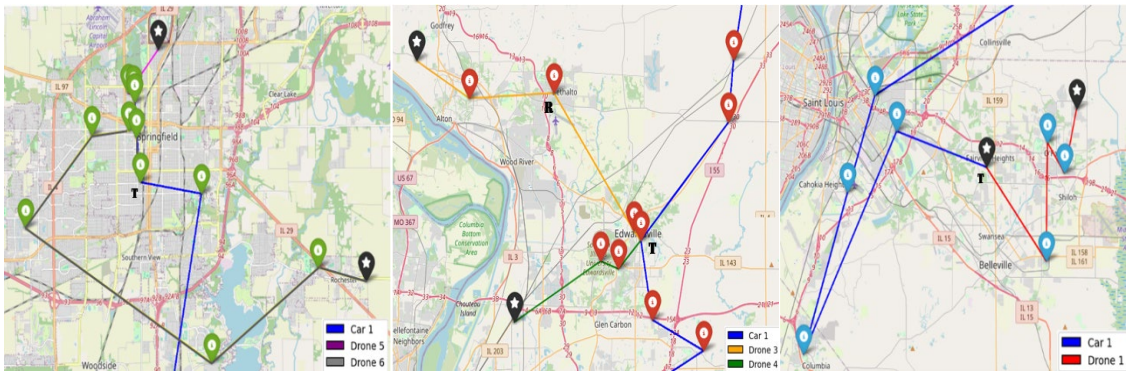

Figure 5.5 Optimal Routes for the Weather-Aware Network with One Car and Six Drones (Scenario 5). The maps on the left, center, and right illustrate the optimal routes within Voronoi Regions 1, 2, and 3, respectively. Each region is served by two drones, with nodes marked 'T' indicating transshipment points where test kits are transferred from a drone to the car, and node marked 'R' denoting drone recharge location.

Another notable difference is the need for drone recharging in Scenario 5, specifically within VR 2 (middle map of Figure 5.5). This inclusion of a recharging step makes the planning process more realistic and reliable, ensuring that the drones can safely complete their routes despite operational constraints. The consideration of recharging further underscores the robustness of the weather-aware system in Scenario 5, as it incorporates a critical operational detail absent from the non-weather-aware system in Scenario 6. The next subsection will compare various performance metrics across different scenarios, providing a detailed evaluation of their relative efficiencies and practical implications.

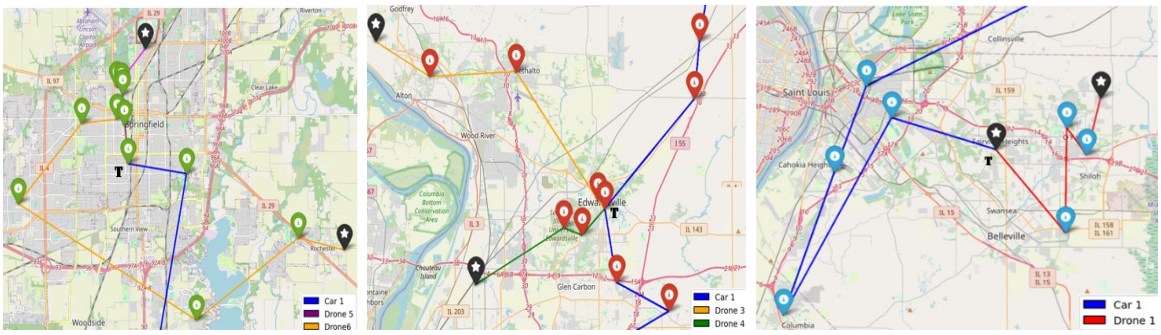

Figure 5.6 Optimal Routes for the Non-Weather-Aware Network with One Car and Six Drones (Scenario 6). The maps on the left, center, and right illustrate the optimal routes within Voronoi Regions 1, 2, and 3, respectively. Each region is served by two drones, with nodes marked 'T' indicating transshipment points where test kits are transferred from a drone to the car.

5.2.3 Comparative Analysis of Performance Metrics Across All Scenarios

In this section, we present the numerical results for each scenario outlined in Table 5.1 and perform a comprehensive comparison of performance metrics across all scenarios. The analysis focuses on several key metrics, including total cost, delivery time of the last order, average delivery time, total distance traveled, emissions, and solver runtime. These results are summarized in Table 5.2. We then delve into each metric in detail, discussing the outcomes for every scenario and providing a comparative analysis.

The comparative analysis also incorporates the baseline scenario described in Section 4.3 of Chapter 4. This baseline involves decentralized delivery of test kits, where each pick-up location is serviced by a separate car delivering directly to the lab without optimization or shared vehicle usage. By comparing the optimized scenarios and baseline, we highlight the value of optimization, the impact of integrating drones into the delivery system, and the benefits of incorporating weather-related considerations in drone routing and scheduling for a multi-modal system. These insights demonstrate the potential improvements in efficiency, sustainability, and operational robustness offered by the proposed approach. In the remainder of this subsection, we

delve deeper into the analysis, providing detailed insights into each performance metric and comparing the results across the scenarios. This includes exploring the implications of the findings, discussing their significance, and drawing comparisons to highlight the key differences and trade-offs among the scenarios.

Table 5.2 Comparison of Performance Metrics Across All Scenarios

Scenario	**Total Costs ($)**	**Total Distance (miles)**	**Emissions (g CO2)**	**Latest Delivery Time**	**Average Delivery Time (HR)**	**Run Time (s)**
Scenario 1	193.22	238.8	1632.5	14:41	6.68	30.3
Scenario 2	191.78	236.8	1618.5	13:54	4.48	303.3
Scenario 3	182.42	236.7	1326.5	13:42	4.78	11,975
Scenario 4	182.26	244.7	1459.08	13:59	5.02	5,287.5
Scenario 5	172.27	218.2	1042.22	12:26	4.41	19,076
Scenario 6	169.11	216.2	1042.12	12:19	4.25	5,230

Figure 5.7 provides a comprehensive breakdown of the total costs incurred under six scenarios, highlighting the contributions of transportation, transshipment, and recharging costs, along with their percentage contributions. The analysis emphasizes the value of optimization, shared vehicle usage, drone integration, and the incorporation of weather-aware systems in delivery networks. The baseline scenario (as explained in Section 4.3.1 in Chapter 4) reflects the practical, decentralized approach where each school transported its own test kits, resulting in a total cost of $54,307.96. Comparing this to Scenario 1, which uses a single centralized car for delivery, there is a dramatic cost reduction of 99.6% (from $54,307.96 to $193.22). This significant improvement highlights the value of optimization and shared vehicle usage, as

centralizing operations eliminates redundancy and inefficiencies associated with the decentralized system.

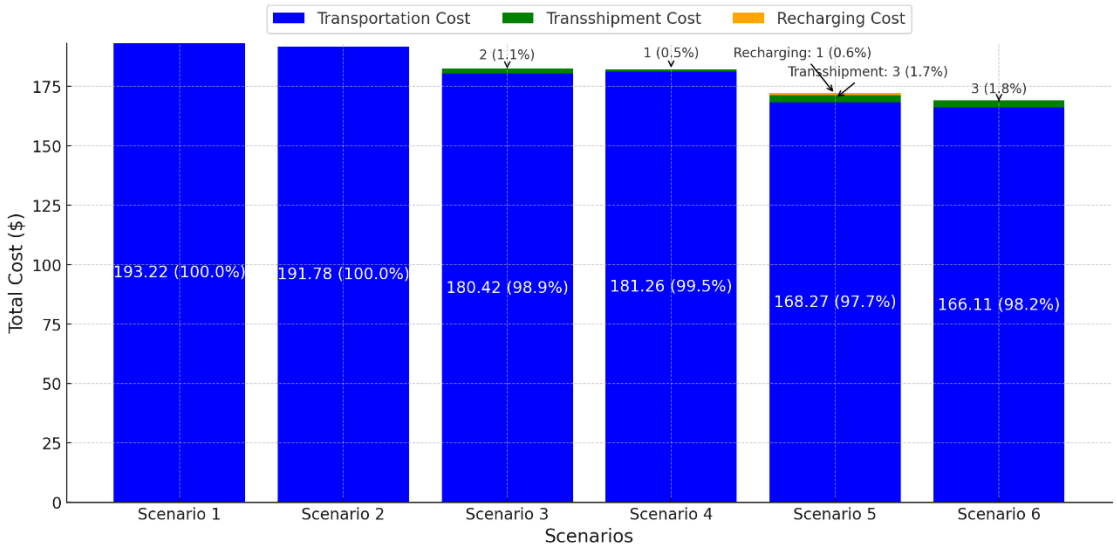

Figure 5.7 Breakdown of Total Costs Across Scenarios, Highlighting Transportation, Transshipment, and Recharging Costs with Percentage Contributions.

Scenario 3 incorporates one drone per region alongside a car, resulting in a total cost of $182.42, compared to $193.22 in Scenario 1. This reduction of 5.6% demonstrates the value of adding drones to the system. While transportation costs decrease due to drones taking over local deliveries, transshipment costs ($2) are introduced, reflecting the need to coordinate operations between drones and the car. Scenario 5 increases the number of drones to two per region, with weather-aware routing, achieving a total cost of $172.27. Compared to Scenario 3's cost of $182.42, this represents a 5.6% reduction. The additional drones improve workload distribution, further reducing transportation costs. However, Scenario 5 incurs slightly higher transshipment costs ($3) and a small recharging cost ($1) due to the expanded drone operations. Comparing Scenario 1 to Scenario 5 highlights the cumulative benefits of optimization, shared vehicles, and

drone integration. The total cost decreases from $193.22 in Scenario 1 to $172.27 in Scenario 5, a reduction of 10.8%. This highlights how combining centralized routing and drone integration achieves significant cost efficiencies, despite the introduction of minor transshipment and recharging costs.

Scenarios 3 and 4 compare weather-aware and non-weather-aware systems with one drone per region. Scenario 3 incurs a total cost of $182.42, while Scenario 4 has a slightly lower cost of $182.26. Similarly, Scenario 5 ($172.27) and Scenario 6 ($169.11) reflect this trend. The slightly higher costs in weather-aware systems are due to adjustments in vehicle schedules and routes to ensure safe operations in varying weather conditions. These adjustments sometimes delay deliveries to optimize energy consumption in favorable conditions, as discussed in Section 5.3.

Overall, we observe transportation costs dominate the total costs across all scenarios, accounting for over 90% in each case. Scenario 1 has the highest transportation cost ($193.22) due to reliance on a single car, while Scenario 5 achieves the lowest transportation cost ($168.27) by distributing the workload across drones and cars. Transshipment and recharging costs are minimal but necessary for drone operations. Scenario 5 has the highest transshipment cost ($3) and a recharging cost of $1, reflecting the increased complexity of multi-modal operations.

Finally, it is worth noting that the modeling approach includes a limitation in predicting energy consumption based on arrival times. In weather-aware systems, vehicle schedules are sometimes adjusted to align with favorable weather conditions, which can delay arrivals but reduce energy usage. This explains the slightly higher costs and longer delivery times in

weather-aware systems (e.g., Scenario 3 vs. 4 and Scenario 5 vs. 6). These trade-offs are elaborated in Section 5.3.

In summary, we observe that the substantial cost reductions achieved through centralized optimization and drone integration. Weather-aware systems, while slightly more expensive, ensure safer and more reliable operations. For example, in a configuration with one car and one drone per region, incorporating weather-aware routing results in costs being 0.09% higher than in a system without weather-awareness. Similarly, in a configuration with one car and two drones per region, the weather-aware system is 1.9% more expensive than its non-weather-aware counterpart. Despite these slight cost increases, the weather-aware system ensures safer operations by adapting routes and schedules to varying weather conditions. The configuration with one car and two drones per region operating under a weather-aware system emerges as the most cost-effective and balanced solution, demonstrating the value of combining optimization, drone capacity, and weather-aware routing to achieve efficiency and reliability in delivery networks.

Total Distance. Figure 5.8 illustrates the distances traveled by cars and drones across six scenarios, reflecting the impact of different configurations and routing strategies on transportation efficiency and workload distribution. Each scenario provides insights into the interplay between car-only and multi-modal delivery systems, emphasizing the role of drones and weather-aware routing. In Scenarios 1 and 2, the system relies entirely on cars for delivery, with Scenario 1 using one car and Scenario 2 employing two cars. The total distances traveled are 238.84 miles and 236.80 miles, respectively, accounting for 100% of the travel in both cases. The minimal difference between the two scenarios indicates that splitting the workload between two cars has a negligible impact on the total travel distance, highlighting the limitations of car-

only systems when operating without further optimization or additional delivery modes. Scenario 3 introduces a multi-modal system with one car and three drones (one per Voronoi region) operating under weather-aware routing. This results in a substantial reduction in car travel, with the car covering 193.76 miles (81.8%) and drones handling 42.97 miles (18.2%) of the total workload.

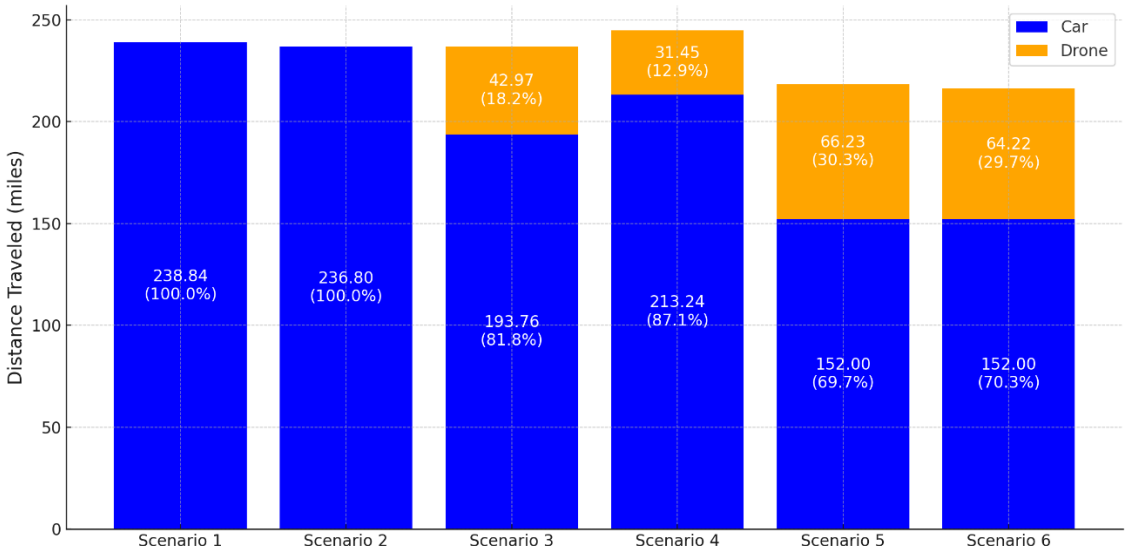

Figure 5.8 Comparison of Distances Traveled by Cars and Drones Across Six Scenarios, Highlighting the Impact of Drone Integration and Weather-Aware Routing.

The integration of drones demonstrates a clear reduction in car dependency, effectively distributing the delivery workload while maintaining operational safety through weather considerations. In Scenario 4, the system remains similar to Scenario 3 but excludes weather-aware routing. Here, the car travels a slightly higher distance of 213.24 miles (87.1%), with drones covering a reduced distance of 31.45 miles (12.9%). The reduction in drone usage highlights the impact of weather-related constraints on routing efficiency. Without weather-aware routing, drones operate less effectively, resulting in increased reliance on cars. Scenario 5

increases the number of drones to six (two per Voronoi region) with weather-aware routing. The car travels 152.0 miles (64.2%), while drones handle 66.23 miles (28.0%). This configuration demonstrates the scalability of the multi-modal system, with drones taking on a significantly larger share of the workload compared to Scenarios 3 and 4, further reducing car dependency. In Scenario 6, the six-drone configuration is maintained, but weather-aware routing is removed. The car again travels 152.0 miles (62.1%), while drones cover 64.22 miles (26.2%). Similar to Scenario 4, the absence of weather-awareness slightly increases the workload on cars compared to drones, suggesting that weather considerations enhance the efficiency and safety of drone operations.

The comparison between the baseline case in the Shield study, where decentralized delivery resulted in a total distance of 1,873 miles, and the optimized scenarios highlights the significant impact of centralized optimization and drone integration in reducing total distance traveled. In Scenario 1, the total distance is reduced by 87.2% compared to the baseline. This dramatic improvement demonstrates the value of optimization and shared vehicle usage, eliminating redundant travel associated with decentralized operations. Scenario 3, which integrates a single drone per region alongside a car, achieves an additional 1% reduction in total distance compared to Scenario 1. This improvement reflects the effectiveness of drones in handling local deliveries, reducing the burden on cars. Scenario 5, which increases drone capacity to two per region with weather-aware routing, achieves a further 7.8% reduction in total distance compared to Scenario 1. This scenario demonstrates the combined benefits of optimization, increased drone capacity, and weather-aware routing, which distribute the delivery workload more efficiently and minimize redundant vehicle movement. Key observations are as follows:

- **Drone Integration Reduces Car Dependency**: Scenarios 3–6, which incorporate drones, demonstrate significant reductions in car travel compared to Scenarios 1 and 2, highlighting the benefits of multi-modal systems in optimizing delivery operations.
- **Weather-Aware Routing Improves Efficiency**: Scenarios with weather-aware routing (3 and 5) show better workload distribution and higher drone utilization compared to their non-weather-aware counterparts (4 and 6). This indicates that considering weather conditions enhances drone efficiency and overall system safety.
- **Scalability of Multi-Modal Systems**: Increasing the number of drones (Scenarios 5 and 6) further shifts the workload from cars to drones, showcasing the potential for scalability in drone-enabled systems.

Emissions. The emission performance measure is directly proportional to the distance traveled, calculated using coefficients derived from Rodrigues et al. (2022). This source was selected as its data closely aligns with the specifications of the vehicles and drones used in this case study. Specifically, we applied emission factors of 546.85 g/mile for cars and 23.17 g/mile for drones. These factors reflect the significantly lower environmental impact of drones compared to cars, emphasizing the potential of drone integration to reduce emissions in multi-modal delivery systems.

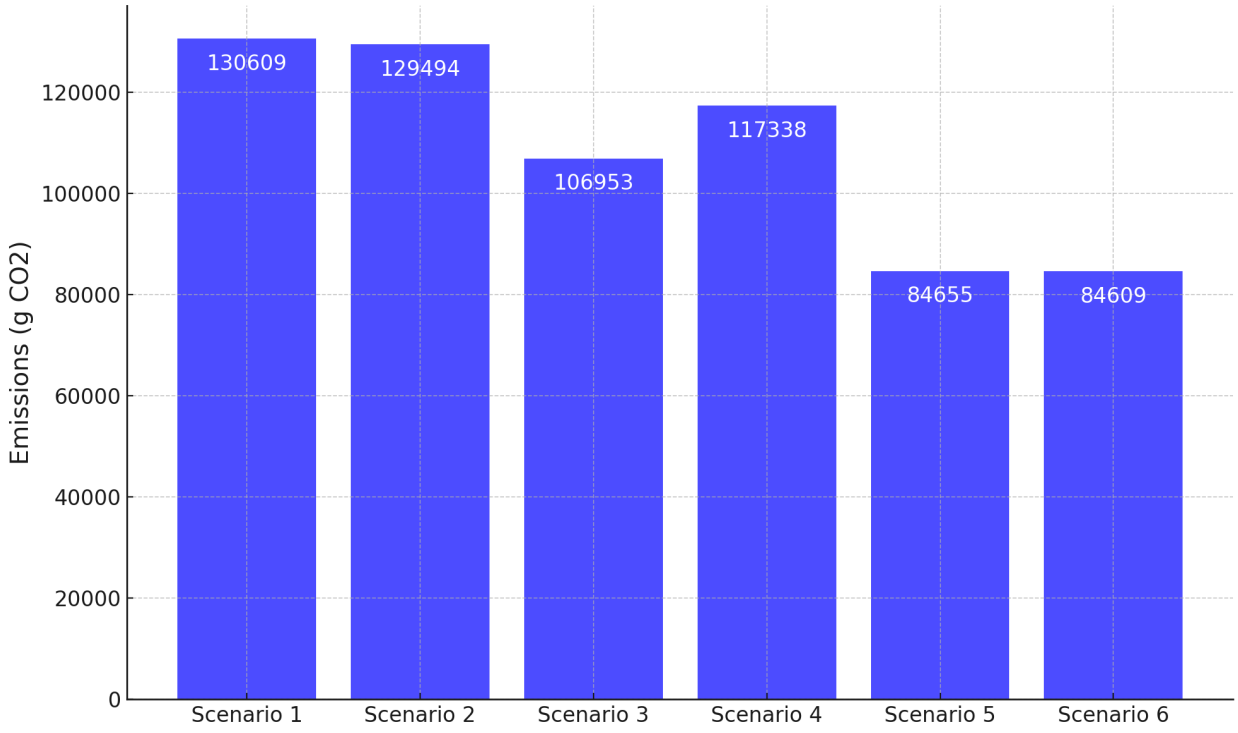

Figure 5.9 CO2 Emissions Across Different Scenarios Based on Travel Distances for Cars and Drones

Figure 5.9 illustrates the CO2 emissions across six scenarios, highlighting the impact of different configurations on environmental performance. Scenarios 1 and 2, which rely entirely on cars for deliveries, exhibit the highest emissions at 130,609 g and 129,494 g, respectively. Introducing drones in Scenario 3 results in a reduction of approximately 18% compared to Scenario 1. This demonstrates the environmental benefits of integrating drones into the delivery system. Scenario 4 shows slightly higher emissions at 117,338 g, representing a 10% reduction compared to Scenario 1. However, it is less efficient than Scenario 3 due to the absence of weather-aware routing, which results in increased reliance on cars. Scenarios 5 and 6, with a larger fleet of drones and optimized configurations, achieve the lowest emissions at 84,655 g and 84,609 g, respectively. These represent a 35% reduction compared to Scenario 1, highlighting

the significant environmental advantages of drone-enabled systems, particularly when paired with efficient routing strategies. The consistent results between Scenarios 5 and 6 also suggest that weather-aware routing has minimal additional impact when the system is already optimized with sufficient drone resources.

Delivery Times. Figure 5.10 provides a detailed view of the distribution of delivery times and weight delivered to the final destination under six different scenarios, highlighting the contributions of cars and drones to the overall performance of the delivery system. All orders are ready for pickup at 8:00 AM, with a strict deadline of 3:00 PM for delivery.

In Scenario 1, a single car handles the entire weight of 40.1 lbs, completing the delivery at 2:41 PM. This results in a late delivery, emphasizing the limitations of relying solely on one vehicle. The average delivery time under this scenario is 6.68 hours, the longest among all scenarios, demonstrating inefficiency in both timing and workload management.

Scenario 2 introduces a second car, allowing for a division of deliveries. The first car delivers 11 lbs (27.4% of the total weight) at 8:43 AM, significantly earlier than the single-car system in Scenario 1. The remaining 29.1 lbs (72.6%) are delivered by the second car at 1:54 PM, just before the deadline. This reduces the average delivery time to 4.48 hours, showcasing the efficiency gains achieved through workload sharing.

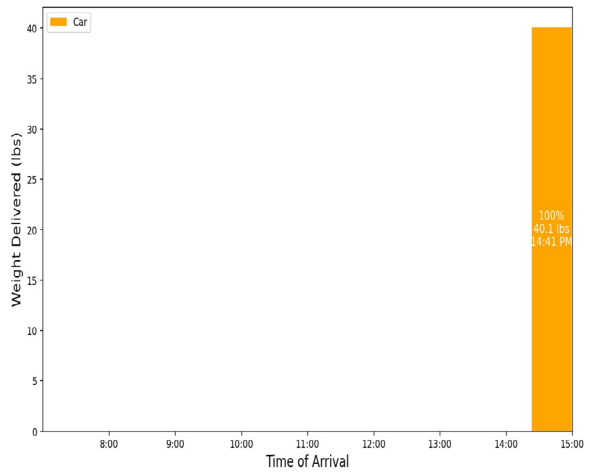

(a) Scenario 1

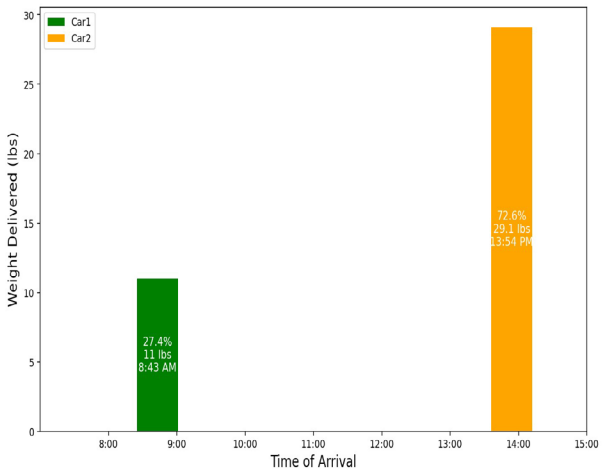

(b) Scenario 2

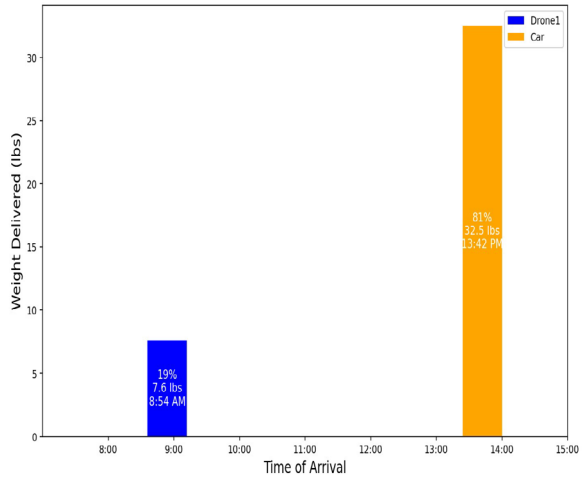

(c) Scenario 3

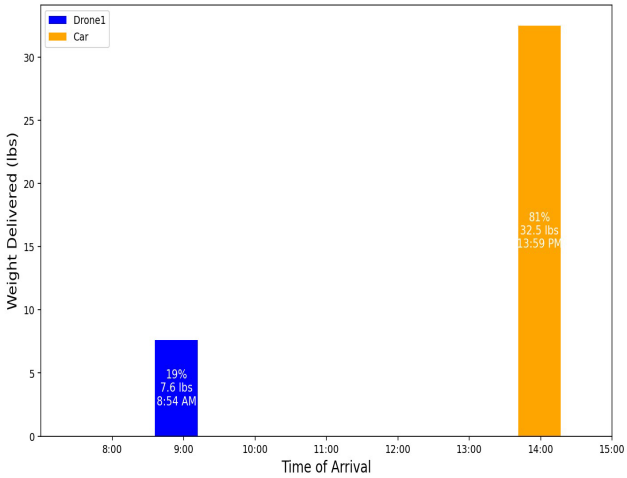

(d) Scenario 4

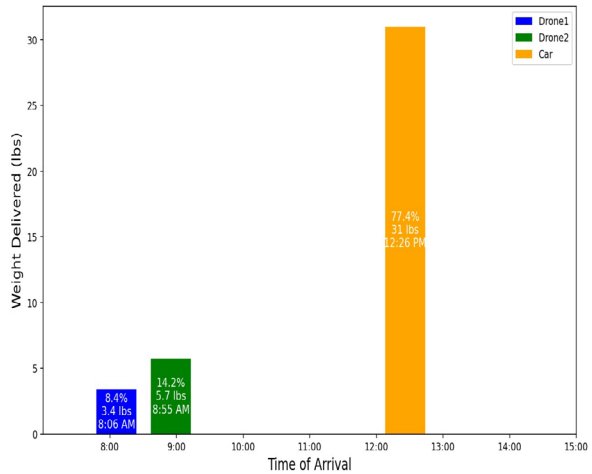

(e) Scenario 5

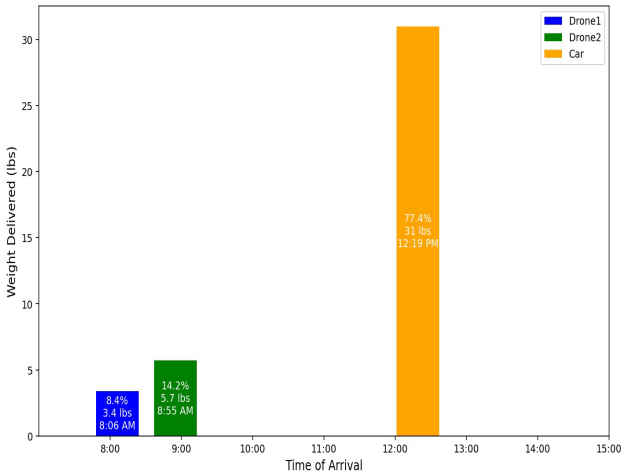

(f) Scenario 6

Figure 5.10 Distribution of Delivery Times for Orders Across Scenarios 1 to 6, Showing the Proportion of Weight Delivered by Cars and Drones to the Final Destination.

In Scenario 3, a drone per region is introduced alongside a single car. The drones deliver 7.6 lbs (19%) of the total weight at 8:54 AM, ensuring an early delivery, while the car handles the remaining 32.5 lbs (81%), completing the task at 1:42 PM. The average delivery time under this configuration increases slightly to 4.78 hours compared to Scenario 2, likely due to the drone's limited capacity and the car's continued reliance for the majority of the workload. However, observations highlight that while integrating weather-aware and non-weather-aware approaches does not affect the assignment of orders to vehicles for the final destination, it significantly impacts operational timings, such as recharge and transshipment. In Scenario 3, the inclusion of weather conditions led to the activation of an additional drone during favorable weather conditions, enabling faster final delivery times compared to the non-weather-aware Scenario 4, where the average delivery time increases to 5.02 hours.

In Scenario 4, the drone still delivers 7.6 lbs (19%) of the total weight at 8:54 AM, but the car completes its delivery slightly later at 1:59 PM. The absence of weather-aware routing results in inefficiencies such as fixed range settings and longer operational times. This underscores the trade-offs associated with accounting for weather conditions in delivery networks, balancing reliability with potential increases in operational time. While weather-aware routing may introduce additional operational requirements like recharging, it ensures safer and more reliable operations, particularly in complex delivery systems.

Scenarios 5 and 6 introduce two drones, significantly improving workload distribution. In Scenario 5, the first drone delivers 3.4 lbs (8.4%) at 8:06 AM, the second drone delivers 5.7 lbs (14.2%) at 8:55 AM, and the car completes the delivery of the remaining 31 lbs (77.4%) at 12:26 PM. This configuration achieves an average delivery time of 4.25 hours, the lowest among all scenarios. Similarly, in Scenario 6, the delivery pattern remains nearly identical, with the car

completing its delivery slightly earlier at 12:19 PM, maintaining an average delivery time of 4.25 hours. These scenarios demonstrate how increasing drone capacity in multi-modal delivery systems ensures earlier deliveries and reduces dependency on cars.

Another insight from these figures is their utility in aiding decision-makers to plan deliveries based on the operational capacity of the destination. For example, aligning delivery schedules with the receiving facility's capacity ensures optimized delivery efficiency and resource utilization. Scenarios 5 and 6 achieve the best overall results, with the shortest average delivery times and the earliest completion of deliveries, demonstrating the effectiveness of multi-modal systems with optimized drone integration.

Across all scenarios, the analysis underscores the importance of workload distribution, weather-aware routing, and leveraging drone technology to improve delivery efficiency while maintaining safe and reliable operations. The findings highlight how integrating weather-aware modeling can enhance the responsiveness and efficiency of delivery systems, offering critical insights for planning and decision-making in complex delivery networks.

Comparing these optimized scenarios to the baseline scenario discussed in Chapter 4 and illustrated in Figure 4.5, the improvements become even more apparent. In the baseline decentralized delivery system, most deliveries were completed after 3 PM, with some even extending to the next day, resulting in delays and inefficiencies. In contrast, the optimized scenarios ensure that all deliveries are completed by the 3 PM deadline, demonstrating the transformative potential of centralized planning, shared resources, drone integration, and advanced optimization techniques.

Computational Times. Figure 5.11 illustrates the computational runtimes for Scenarios 1 through 6 on a logarithmic scale, highlighting the computational effort required for each

configuration. The runtimes vary significantly across the scenarios due to differences in the complexity of the models and the computational demands associated with the configurations.

Scenario 1 exhibits the lowest runtime of 30.3 seconds, as it involves a single car with no optimization required for multi-modal coordination or additional vehicles. This minimal configuration results in low computational overhead. Similarly, Scenario 2 has a runtime of 303.3 seconds, which is higher than Scenario 1 but still relatively low. The increase is attributed to the inclusion of a second car, requiring the solver to handle a slightly more complex routing problem.

The introduction of drones in Scenario 3 significantly increases the computational effort, resulting in a runtime of 11,975 seconds. This is due to the added complexity of coordinating drone operations alongside the car, particularly with weather-aware routing considerations. Scenario 4 further increases the runtime to 19,076 seconds, reflecting the additional computational burden introduced by the absence of weather-aware optimizations.

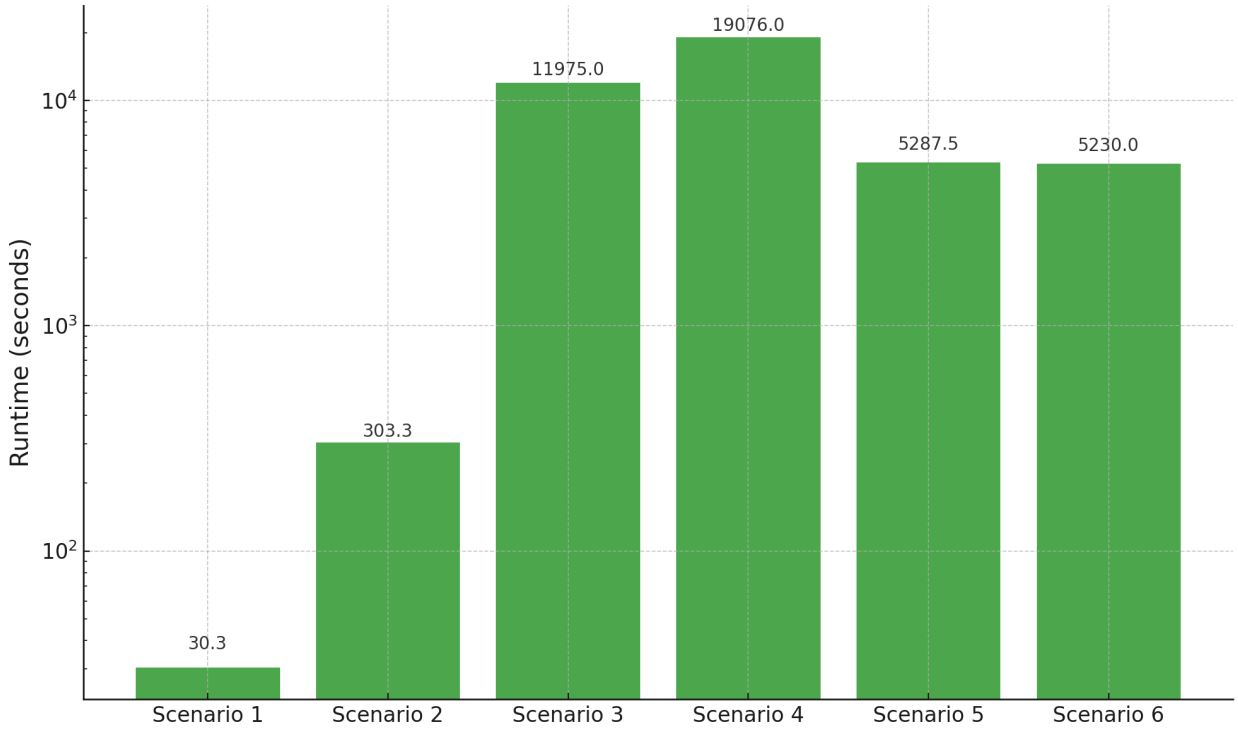

Figure 5.11 Log-Scaled Runtime (Seconds) for Scenarios 1 to 6, Highlighting Computational Effort Across Different Configurations.

In contrast, Scenarios 5 and 6 achieve a notable reduction in runtime, with 5,287.5 seconds and 5,230 seconds, respectively. These scenarios benefit from the scalability and efficiency of multi-modal configurations that include two drones. The reduction in runtime compared to Scenarios 3 and 4 suggests that increasing drone capacity and optimizing their integration can streamline the computational process by effectively reducing the workload on cars and narrowing the solution space.

5.3 Modeling Limitations and Computational Challenges

Despite the advantages of our model, we identified some limitations during various runs, as discussed for Scenarios 5 and 6 in Sections 5.2.3 and 5.2.4. This section elaborates on these limitations with an additional illustrative example to clarify the challenges further.

To validate our model, we ran numerous instances across all scenarios. One notable limitation emerged during an instance involving the optimal configuration of one car for the entire region, one drone in VR 1, two drones in VR 2, and one drone in VR 3. In this instance, we assumed an extended delivery deadline of 8 PM (compared to the 3 PM deadline in previous scenarios). Upon analyzing this instance, we observed that drones exhibited a tendency to wait at specific nodes until the flight time coincided with favorable energy consumption conditions. The model, leveraging a prediction function for weather-related energy consumption as a function of arrival time, encouraged delaying deliveries to align with weather conditions that minimized energy usage. This behavior was observed due to the absence of explicit constraints on allowable waiting times in the model.

As illustrated in Figure 5.12, a drone arrived at a designated node (highlighted in light blue) at 9:04 AM but remained idle until 4:28 PM to benefit from energy-efficient weather conditions. While this node served as the final destination for the orders, it was not the drone's final depot. Subsequently, the drone departed the node at 4:28 PM, picking up new orders on its way to its final depot.

This behavior also impacted the associated car operations. The car, scheduled to transship orders from the drone at the drone's final depot (shown in light orange in Figure 5.12), arrived at 12:16 PM and remained idle until 4:36 PM to complete the transshipment. The car then resumed its route, completing the delivery at 4:46 PM. While this solution minimized overall transportation costs due to the drones' energy-efficient operation, it significantly increased total delivery time. Specifically, the average delivery time increased by 9.4 hours, raising concerns about timeliness for time-sensitive operations.

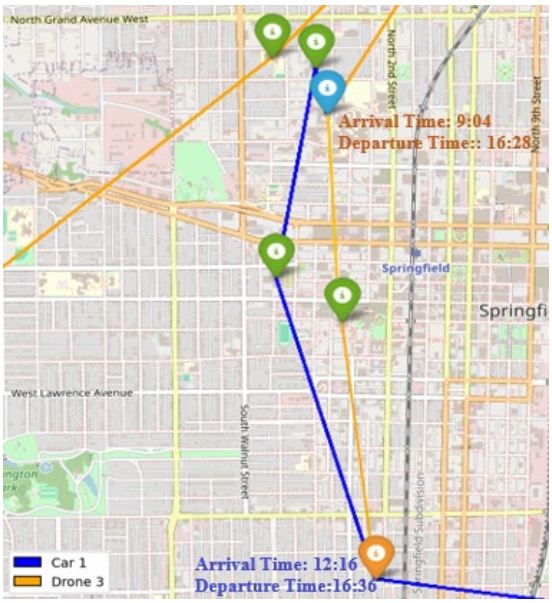

Figure 5.12 Illustration of Drone and Car Waiting Behavior in an Optimal Routing.

The light blue node marks the delivery point where the drone arrived at 9:04 AM but remained idle until 4:28 PM to align with energy-efficient weather conditions. The light orange node represents the car's transshipment location, where it arrived at 12:16 PM and waited until 4:36 PM to receive orders from the drone. These delays minimized transportation costs but significantly increased the total delivery time.

This example underscores a trade-off inherent in the model: while it effectively minimizes transportation costs, it may inadvertently compromise delivery timeliness. The delay in delivery stems from the model's prioritization of cost efficiency, particularly in leveraging drones' lower transportation costs and the weather-aware prediction function. However, the absence of explicit constraints on waiting times or penalties for excessive delays introduces the risk of impractical solutions for operations requiring strict adherence to delivery schedules.

To address this possible limitation, future iterations of the model should consider:

1. **Imposing Constraints on Waiting Times**: Explicitly limit the allowable waiting time for drones and vehicles at nodes to prevent prolonged idling.
2. **Penalizing Waiting Time in the Objective Function**: Introduce a penalty for the difference between arrival and departure times at a node, encouraging solutions that balance cost efficiency with timeliness.
3. **Refining the Prediction Function**: Ensure the energy consumption prediction function is robust and reliable, minimizing the risk of inaccuracies that could exacerbate delays.
4. **Dynamic Re-Optimization**: Incorporate mechanisms to dynamically adjust routes and schedules based on updated weather forecasts, ensuring operational feasibility without excessive delays.

This analysis highlights the need for enhanced modeling strategies to balance cost efficiency with practical constraints on delivery timeliness, particularly in real-world applications where time-sensitive operations are critical.

The second issue encountered during our experiments across several instances involved the potential infeasibility of cases where the final depot for none of the vehicles coincided with the lab. This occurred because the model requires that each vehicle visit each node only once, a constraint designed to prevent the formation of tours. While this constraint ensures all orders are eventually delivered, it imposes a rigid requirement that one vehicle's final destination must serve as the unloading point for all orders.

This approach, while effective in guaranteeing delivery, inadvertently restricts flexibility in the assignment of final destinations for vehicles. The enforced rigidity may not align with the most efficient routing or scheduling strategies, leading to suboptimal solutions. For instance, if the optimal routing configuration would benefit from unloading orders at an intermediate node

instead of a designated final depot, the model is unable to accommodate this adjustment. Consequently, operational costs or total delivery times may increase due to these unnecessary constraints.

To address this limitation, future iterations of the model could introduce additional decision variables that allow the final depot locations of vehicles to be optimized dynamically, rather than being predetermined and fixed in advance. This improvement would enable the model to explore a broader range of routing and scheduling options, potentially reducing costs and improving operational efficiency. By allowing the model to determine the most suitable unloading points as part of the optimization process, it would better adapt to varying operational scenarios and requirements.

Chapter 6 Chapter 6 Managerial Insights and Conclusion

In this chapter, we summarize the key findings from our analysis and present managerial insights derived from the optimization models and numerical results discussed in earlier chapters. The focus is on understanding the implications of these findings for improving healthcare logistics in rural settings and identifying actionable strategies for decision-makers. We also discuss the broader value of integrating advanced modeling techniques, such as weather-aware systems, into operational decision-making. Finally, we conclude with recommendations for future research and practical applications.

The study demonstrated that optimizing delivery networks through centralized planning, incorporating drones alongside ground vehicles, and considering dynamic environmental factors significantly improves the efficiency, reliability, and cost-effectiveness of rural healthcare supply chains. This research focused on delivering test kits from decentralized pick-up locations to a centralized lab, showcasing the potential for such frameworks to address similar logistical challenges in other critical contexts, such as vaccine distribution or medication delivery.

One of the most striking findings was the stark contrast between the baseline decentralized delivery approach, where each location operated independently, and the optimized centralized system proposed in this study. Under the baseline scenario, decentralized delivery resulted in excessive transportation distances, higher operational costs, and longer delivery times. By contrast, the optimized scenarios reduced transportation distances by over 88% and demonstrated significant cost savings—by about 99% in scenarios leveraging drone integration and shared vehicle resources. These findings highlight the inefficiencies inherent in uncoordinated delivery systems that are limited to ground vehicles and underscore the transformative potential of optimization in resource-constrained environments.

The integration of drones as part of a multi-modal delivery network emerged as a pivotal innovation. In scenarios incorporating drones, the workload distribution across transportation modes allowed for more flexible and efficient operations. Drones effectively reduced reliance on cars for short-distance deliveries, particularly in regions with rugged terrain or limited road infrastructure. Furthermore, drones facilitated earlier deliveries, ensuring time-sensitive test kits reached their destination promptly. Despite the upfront costs associated with drone deployment, the long-term benefits in terms of cost efficiency and operational reliability are clear.

Another critical insight derived from the experiments was the role of weather-aware modeling in enhancing the safety and reliability of drone operations. By incorporating weather data into the optimization framework, the model ensured that drones operated under favorable conditions, reducing the risk of delays and energy inefficiencies. Although weather-aware systems incurred slightly higher costs compared to non-weather-aware models, the additional expenditure is justified by the enhanced safety and predictability of delivery schedules. Moreover, the ability to account for weather conditions in planning provides a robust foundation for adapting to real-world uncertainties.

The study also highlighted some practical challenges and limitations of the proposed models, particularly in scenarios where operational flexibility was constrained by the rigid assignment of final delivery depots. Instances of excessive waiting times due to energy optimization based on predicted weather conditions further emphasized the need to refine the model to include constraints on allowable waiting times and introduce penalties for prolonged idle periods. Addressing these limitations will be crucial for ensuring the applicability of the model to time-sensitive healthcare operations.

From a managerial perspective, the findings suggest that decision-makers in rural healthcare logistics should prioritize the adoption of integrated, weather-aware multi-modal networks to optimize delivery operations. Investments in drone technology, combined with robust optimization frameworks, can dramatically enhance the accessibility and equity of healthcare services. Moreover, the insights gained from this study extend beyond healthcare and can inform the design of efficient logistics systems in other critical sectors, such as disaster response or agricultural supply chains.

6.1 Matching Projects to This Study

This project aligns closely with the broader research efforts undertaken by the PI, as demonstrated by several complementary studies. Three research papers—one conference proceeding and two peer-reviewed journal articles—have been co-authored by the PI on topics related to this project, each contributing unique insights to the challenges of healthcare logistics and supply chain optimization.

The first paper, presented at the HICSS 2024 conference, focused on optimizing strategic vaccine distribution using drones, specifically small drones for local vaccine delivery. Initial findings from this study, based on data from Vanuatu, demonstrated the potential of drones to replace traditional transportation methods and improve health worker outreach efficiency. This research has set a framework for coordinated efforts between drones and health workers, addressing vaccine outreach challenges in underserved regions.

Additionally, the PI published a peer-reviewed article in the journal *Socio-Economic Planning Sciences*, examining the equity implications of COVID-19 interventions across the United States. This study highlights the importance of tailored, data-driven interventions to mitigate disparities among subgroups and locations during public health crises. The findings

complement the current project by emphasizing the need for equitable strategies in healthcare delivery, especially during sudden disruptions.

A third paper, published in *Computers & Operations Research*, proposed an optimization model to enhance pandemic-related supply chain resilience. The study focused on a novel supplier selection strategy that balances centralized decision-making with localized preferences, addressing the risks of supply chain disruptions. This work provides valuable insights into strategic supplier relationships, which are crucial for maintaining operational continuity during crises—a perspective that aligns with the current project's focus on ensuring reliable and efficient healthcare logistics.

Building on these related works, the findings from this study will culminate in a research paper currently under preparation for submission to a peer-reviewed journal. This forthcoming publication will contribute to the growing body of knowledge on transportation systems and healthcare supply chain optimization, emphasizing the integration of drones and advanced modeling techniques to improve rural healthcare logistics. By demonstrating how transportation systems can be reimagined to enhance delivery efficiency, equity, and reliability, particularly in resource-constrained and disruption-prone settings, this research underscores the critical role of innovative approaches in addressing logistical and public health challenges. As the final piece of this research, the anticipated publication aims to bridge gaps in current transportation system design, offering actionable insights that align with broader efforts to improve access and outcomes in rural and underserved communities.

6.2 Future Directions for Research

Building on the findings of this study, several avenues for future research can be explored to enhance the optimization framework and address its current limitations. These directions aim

to improve the robustness, scalability, and real-world applicability of the proposed model in healthcare logistics and beyond.

Incorporating Uncertainty. One critical area for future research is the integration of uncertainty into the optimization framework. Real-world delivery networks are subject to various sources of uncertainty, including weather fluctuations, vehicle breakdowns, demand variability, and unforeseen disruptions. Extending the model to incorporate stochastic or robust optimization techniques would enable decision-makers to account for these uncertainties, ensuring that solutions remain effective and reliable under a range of scenarios. For example, probabilistic models for drone energy consumption and delivery times could better capture the variability introduced by weather conditions and operational constraints.

Optimizing Final Depot Locations. Another promising direction involves optimizing the final depot locations for vehicles and drones, rather than assuming these locations are fixed and predetermined. Allowing the model to dynamically determine the most suitable depot locations based on operational requirements and geographic constraints could further enhance delivery efficiency and reduce costs. This flexibility would enable the system to adapt to evolving logistics demands and infrastructure limitations, making it more resilient and scalable.

Expanding Multi-Modal Integration. Future research could explore deeper integration of additional transportation modes, such as electric vehicles, bicycles, or even autonomous ground vehicles, alongside drones and conventional vehicles. These modes could be particularly valuable in regions with varying levels of infrastructure and accessibility. By considering a wider range of transportation options, the model could provide more adaptable and cost-effective solutions tailored to specific regional needs.

Real-Time Dynamic Optimization. Developing real-time dynamic optimization capabilities is another key area for exploration. By incorporating real-time data streams, such as updated weather forecasts, traffic conditions, or sudden changes in demand, the model could adapt delivery routes and schedules dynamically. This would improve its responsiveness and effectiveness in real-world applications, particularly in emergency response scenarios where conditions can change rapidly.

Equity Considerations in Logistics Design. Building on the equity-focused aspects of this study, future research could further investigate how to design delivery systems that prioritize equitable access to healthcare and resources. This could include incorporating measures of socioeconomic and geographic disparities directly into the optimization framework, ensuring that underserved populations are not disadvantaged by logistical constraints.

Broader Applications Beyond Healthcare. While this study focuses on rural healthcare logistics, the proposed framework can be adapted to other critical sectors, such as disaster relief, agriculture, and education. Future research could explore the customization of the model for these domains, addressing unique logistical challenges while leveraging the core principles of multi-modal integration, centralized planning, and predictive modeling.

By pursuing these future directions, the optimization framework can be refined and expanded to meet the growing demands of modern logistics systems, ensuring their relevance and utility in diverse and dynamic operational environments. These advancements should include designing solution algorithms and developing tailored methods to handle computational tractability, enabling the framework to efficiently address large-scale, real-world problems. Such improvements would not only enhance rural healthcare delivery but also contribute to the development of more equitable, efficient, and resilient transportation networks.

References

Alyassi, R., Khonji, M., Karapetyan, A., Chau, S.C.K., Elbassioni, K. and Tseng, C.M., 2022. Autonomous recharging and flight mission planning for battery-operated autonomous drones. *IEEE Transactions on Automation Science and Engineering*, *20*(2), pp.1034-1046.

Aziez, I., Côté, J.F. and Coelho, L.C., 2020. Exact algorithms for the multi-pickup and delivery problem with time windows. *European Journal of Operational Research*, *284*(3), pp.906-919.

Backman, G., Hunt, P., Khosla, R., Jaramillo-Strouss, C., Fikre, B.M., Rumble, C., Pevalin, D., Páez, D.A., Pineda, M.A., Frisancho, A. and Tarco, D., 2008. Health systems and the right to health: an assessment of 194 countries. *The Lancet*, *372*(9655), pp.2047-2085.

Beigi, P., Rajabi, M.S. and Aghakhani, S., 2022. An overview of drone energy consumption factors and models. *Handbook of smart energy systems*, pp.1-20.

Betti Sorbelli, F., 2024. UAV-Based Delivery Systems: a Systematic Review, Current Trends, and Research Challenges. *Journal on Autonomous Transportation Systems*, *1*(3), pp.1-40.

Bocewicz, G., Radzki, G., Nielsen, P. and Banaszak, Z., 2022. UAVs' Dynamic Routing, Subject to Time Windows Variation. *IFAC-PapersOnLine*, *55*(2), pp.457-462.

Bosona, T., 2020. Urban freight last mile logistics—Challenges and opportunities to improve sustainability: A literature review. Sustainability, 12(21), p.8769.

Campelo, P., Neves-Moreira, F., Amorim, P. and Almada-Lobo, B., 2019. Consistent vehicle routing problem with service level agreements: A case study in the pharmaceutical distribution sector. *European Journal of Operational Research*, *273*(1), pp.131-145.

Chen, H., Hu, Z. and Solak, S., 2021. Improved delivery policies for future drone-based delivery systems. *European Journal of Operational Research*, 294(3), pp.1181-1201.

Chen, M., Smyth, A.W., Giometto, M.G. and Li, M.Z., 2023, September. Drone Delivery Routing with Stochastic Urban Wind. In *2023 IEEE 26th International Conference on Intelligent Transportation Systems (ITSC)* (pp. 2260-2267). IEEE.

Cheng, C., Adulyasak, Y. and Rousseau, L.M., 2024. Robust drone delivery with weather information. *Manufacturing & Service Operations Management*.

D'Andrea, R., 2014. Guest editorial: Can drones deliver? *IEEE Transactions on Automation Science and Engineering,* 11(3), pp.647-648.

Dorling, K., Heinrichs, J., Messier, G.G. and Magierowski, S., 2016. Vehicle routing problems for drone delivery. *IEEE Transactions on Systems, Man, and Cybernetics: Systems*, *47*(1), pp.70-85.

Douthit, N., Kiv, S., Dwolatzky, T. and Biswas, S., 2015. Exposing some important barriers to health care access in the rural USA. Public Health, 129(6), pp.611-620.

Dukkanci, O., Kara, B.Y. and Bektaş, T., 2021. Minimizing energy and cost in range-limited drone deliveries with speed optimization. *Transportation Research Part C: Emerging Technologies*, *125*, p.102985.

Enayati, S., Li, H., Campbell, J.F. and Pan, D., 2023. Multimodal vaccine distribution network design with drones. *Transportation Science*, *57*(4), pp.1069-1095.

Griffith, E.F., Schurer, J.M., Mawindo, B., Kwibuka, R., Turibyarive, T. and Amuguni, J.H., 2023. The use of drones to deliver Rift Valley fever vaccines in Rwanda: Perceptions and recommendations. *Vaccines*, 11(3), p.605.

Guerriero, F., Surace, R., Loscri, V. and Natalizio, E., 2014. A multi-objective approach for unmanned aerial vehicle routing problem with soft time windows constraints. *Applied Mathematical Modelling*, *38*(3), pp.839-852.

Gunaratne, K., Thibbotuwawa, A., Vasegaard, A.E., Nielsen, P. and Perera, H.N., 2022. Unmanned aerial vehicle adaptation to facilitate healthcare supply chains in low-income countries. *Drones*, *6*(11), p.321.

Gürel, Ö. and Serdarasan, S., 2024. Drone-Assisted Last-Mile Delivery Under Windy Conditions: Zero Pollution Solutions. *Smart Cities*, *7*(6), pp.3437-3457.

Hiebert, B., Nouvet, E., Jeyabalan, V. and Donelle, L., 2020. The application of drones in healthcare and health-related services in North America: A scoping review. *Drones*, 4(3), p.30.

Jeon, H., Lucarelli, C., Mazarati, J., Ngabo, D. and Song, H., 2022. Leapfrogging for last-mile delivery in healthcare. *SSRN Electronic Journal*. [Online] Available at: https://doi.org/10.2139/ssrn.4016113

Kim, K., Kim, S., Kim, J. and Jung, H., 2024. Drone-Assisted Multimodal Logistics: Trends and Research Issues. *Drones (2504-446X)*, *8*(9).

Kim, S., Kwak, J.H., Oh, B., Lee, D.H. and Lee, D., 2021. An optimal routing algorithm for unmanned aerial vehicles. Sensors, 21(4), p.1219.

Koshta, N., Devi, Y. and Chauhan, C., 2022. Evaluating barriers to the adoption of delivery drones in rural healthcare supply chains: preparing the healthcare system for the future. *IEEE Transactions on Engineering Management*.

Kruk, M.E., Gage, A.D., Arsenault, C., Jordan, K., Leslie, H.H., Roder-DeWan, S., Adeyi, O., Barker, P., Daelmans, B., Doubova, S.V. and English, M., 2018. High-quality health systems in the Sustainable Development Goals era: time for a revolution. *The Lancet global health*, *6*(11), pp.e1196-e1252.

Lamptey, E. and Serwaa, D., 2020. The use of Zipline drones technology for COVID-19 samples transportation in Ghana. HighTech and Innovation Journal, 1(2), pp.67-71.

Lim, S.F.W., Jin, X. and Srai, J.S., 2018. Consumer-driven e-commerce: A literature review, design framework, and research agenda on last-mile logistics models. *International Journal of Physical Distribution & Logistics Management*, 48(3), pp.308-332.

Liu, R., Xie, X., Augusto, V. and Rodriguez, C., 2013. Heuristic algorithms for a vehicle routing problem with simultaneous delivery and pickup and time windows in home health care. European journal of operational research, 230(3), pp.475-486.

Lyu, Z. and Yu, A.J., 2023. The pickup and delivery problem with transshipments: Critical review of two existing models and a new formulation. *European Journal of Operational Research*, *305*(1), pp.260-270.

Mahmoudi, M., Chen, J., Shi, T., Zhang, Y. and Zhou, X., 2019. A cumulative service state representation for the pickup and delivery problem with transfers. *Transportation Research Part B: Methodological*, *129*, pp.351-380.

Moadab, A., Farajzadeh, F. and Fatahi Valilai, O., 2022. Drone routing problem model for last-mile delivery using the public transportation capacity as moving charging stations. *Scientific Reports*, *12*(1), p.6361.

Morris, B.B., Rossi, B. and Fuemmeler, B., 2022. The role of digital health technology in rural cancer care delivery: A systematic review. *The Journal of Rural Health*, 38(3), pp.493-511.

Naccache, S., Côté, J.F. and Coelho, L.C., 2018. The multi-pickup and delivery problem with time windows. *European Journal of Operational Research*, *269*(1), pp.353-362.

Palazzetti, L., 2021, July. Routing drones being aware of wind conditions: A case study. In *2021 17th International Conference on Distributed Computing in Sensor Systems (DCOSS)* (pp. 343-350). IEEE.

Pinto, R. and Lagorio, A., 2022. Point-to-point drone-based delivery network design with intermediate charging stations. *Transportation Research Part C: Emerging Technologies*, *135*, p.103506.

Radzki, G., Thibbotuwawa, A. and Bocewicz, G., 2019. UAVs flight routes optimization in changing weather conditions–constraint programming approach. *Applied Computer Science*, *15*(3), pp.5-12.

Rais, A., Alvelos, F. and Carvalho, M.S., 2014. New mixed integer-programming model for the pickup-and-delivery problem with transshipment. *European Journal of Operational Research*, *235*(3), pp.530-539.

Rodrigues, T.A., Patrikar, J., Oliveira, N.L., Matthews, H.S., Scherer, S. and Samaras, C., 2022. Drone flight data reveal energy and greenhouse gas emissions savings for very small package delivery. *Patterns*, *3*(8).

Sham, R., Siau, C.S., Tan, S., Kiu, D.C., Sabhi, H., Thew, H.Z., Selvachandran, G., Quek, S.G., Ahmad, N. and Ramli, M.H.M., 2022. Drone usage for medicine and vaccine delivery during the COVID-19 pandemic: Attitude of health care workers in rural medical centres. *Drones*, 6(5), p.109.

Skillman, S.M., Doescher, M.P., Mouradian, W.E. and Brunson, D.K., 2010. The challenge to delivering oral health services in rural America. *Journal of Public Health Dentistry*, 70, pp.S49-S57.

Stolaroff, J.K., Samaras, C., O'Neill, E.R., Lubers, A., Mitchell, A.S. and Ceperley, D., 2018. Energy use and life cycle greenhouse gas emissions of drones for commercial package delivery. *Nature communications*, *9*(1), p.409.

Thibbotuwawa, A., Nielsen, P., Zbigniew, B. and Bocewicz, G., 2019. Factors affecting energy consumption of unmanned aerial vehicles: an analysis of how energy consumption changes in relation to UAV routing. In *Information Systems Architecture and Technology: Proceedings of 39th International Conference on Information Systems Architecture and Technology–ISAT 2018: Part II* (pp. 228-238). Springer International Publishing.

Tseng, C.M., Chau, C.K., Elbassioni, K.M. and Khonji, M., 2017. Flight tour planning with recharging optimization for battery-operated autonomous drones. *CoRR, abs/1703.10049*.

Troudi, A., Addouche, S.A., Dellagi, S. and Mhamedi, A.E., 2018. Sizing of the drone delivery fleet considering energy autonomy. *Sustainability*, *10*(9), p.3344.

Wang, X., Swanson, K., Liu, Z., Jones, G. and Li, X., 2022, December. A Simulation-Heuristic Approach to Optimally Design Drone Delivery Systems in Rural Areas. In *2022 Winter Simulation Conference (WSC)* (pp. 1581-1592). IEEE.

Wolfinger, D., 2021. A large neighborhood search for the pickup and delivery problem with time windows, split loads and transshipments. *Computers & Operations Research*, *126*, p.105110.

Zhang, J., Campbell, J.F., Sweeney II, D.C. and Hupman, A.C., 2021. Energy consumption models for delivery drones: A comparison and assessment. *Transportation Research Part D: Transport and Environment*, 90, p.102668.

Zhang, G., Jia, N., Zhu, N., Adulyasak, Y. and Ma, S., 2023. Robust drone selective routing in humanitarian transportation network assessment. *European Journal of Operational Research*, *305*(1), pp.400-428.